Title
Spatial distribution of isoprene emissions from North America derived from formaldehyde column measurements by the OMI satellite sensor

Journal
Journal of Geophysical Research, 113(D2)

ISSN
0148-0227

Authors
Millet, Dylan B
Jacob, Daniel J
Boersma, K Folkert
et al.

Publication Date
2008

DOI
10.1029/2007jd008950

Spatial distribution of isoprene emissions from North America derived from formaldehyde column measurements by the OMI satellite sensor

Dylan B. Millet,[1,5] Daniel J. Jacob,[1] K. Folkert Boersma,[1] Tzung-May Fu,[1] Thomas P. Kurosu,[2] Kelly Chance,[2] Colette L. Heald,[3,6] and Alex Guenther[4]

Received 10 May 2007; revised 19 September 2007; accepted 25 October 2007; published 26 January 2008.

[1] Space-borne formaldehyde (HCHO) column measurements from the Ozone Monitoring Instrument (OMI), with 13 × 24 km^2 nadir footprint and daily global coverage, provide new constraints on the spatial distribution of biogenic isoprene emission from North America. OMI HCHO columns for June-August 2006 are consistent with measurements from the earlier GOME satellite sensor (1996–2001) but OMI is 2–14% lower. The spatial distribution of OMI HCHO columns follows that of isoprene emission; anthropogenic hydrocarbon emissions are undetectable except in Houston. We develop updated relationships between HCHO columns and isoprene emission from a chemical transport model (GEOS-Chem), and use these to infer top-down constraints on isoprene emissions from the OMI data. We compare the OMI-derived emissions to a state-of-science bottom-up isoprene emission inventory (MEGAN) driven by two land cover databases, and use the results to optimize the MEGAN emission factors (EFs) for broadleaf trees (the main isoprene source). The OMI-derived isoprene emissions in North America (June–August 2006) with 1° × 1° resolution are spatially consistent with MEGAN (R^2 = 0.48–0.68) but are lower (by 4–25% on average). MEGAN overestimates emissions in the Ozarks and the Upper South. A better fit to OMI (R^2 = 0.73) is obtained in MEGAN by using a uniform isoprene EF from broadleaf trees rather than variable EFs. Thus MEGAN may overestimate emissions in areas where it specifies particularly high EFs. Within-canopy isoprene oxidation may also lead to significant differences between the effective isoprene emission to the atmosphere seen by OMI and the actual isoprene emission determined by MEGAN.

Citation: Millet, D. B., D. J. Jacob, K. F. Boersma, T. M. Fu, T. P. Kurosu, K. Chance, C. L. Heald, and A. Guenther (2008), Spatial distribution of isoprene emissions from North America derived from formaldehyde column measurements by the OMI satellite sensor, *J. Geophys. Res.*, *113*, D02307, doi:10.1029/2007JD008950.

1. Introduction

[2] Isoprene (C_5H_8) is the principal non-methane volatile organic compound (VOC) emitted from vegetation. Global emissions are estimated at 220–750 Tg a^{-1} [*Granier et al.*, 2000; *Poisson et al.*, 2000; *Bey et al.*, 2001; *Ehhalt and Prather*, 2001; *Levis et al.*, 2003; *Shim et al.*, 2005; *Guenther et al.*, 2006], comparable to those of methane (500–600 Tg a^{-1}) [*Hein et al.*, 1997; *Wuebbles and Hayhoe*, 2002; *Mikaloff Fletcher et al.*, 2004; *Wang et al.*, 2004; *Chen and Prinn*, 2006], and several times greater than all anthropogenic VOCs combined (100–200 Tg a^{-1}) [*Müller*, 1992; *Olivier and Berdowski*, 2001]. Isoprene is highly reactive, with an atmospheric lifetime against oxidation by OH of typically less than 1 h, and is an important source of tropospheric ozone [*Trainer et al.*, 1987] and secondary organic aerosol [*Henze and Seinfeld*, 2006; *Kroll et al.*, 2006], as well as a sink of OH [*Jacob and Wofsy*, 1988]. Bottom-up isoprene emission estimates based on leaf, plant, and ecosystem level measurements suffer from the uncertainties inherent in extrapolating such data to larger scales, and from a paucity of measurements over much of the world. Formaldehyde (HCHO) is produced in high yield during isoprene oxidation and can be measured from space in the near-UV by solar backscatter instruments [*Chance et al.*, 2000]. Here we use HCHO columns (Ω_{HCHO}) measured from the Dutch-Finnish Ozone Monitoring Instrument (OMI) [*Levelt et al.*, 2006], aboard NASA's Aura satellite, to constrain the spatial distribution of isoprene emissions

[1]Department of Earth and Planetary Sciences and School of Engineering and Applied Sciences, Harvard University, Cambridge, Massachusetts, USA.
[2]Harvard-Smithsonian Center for Astrophysics, Cambridge, Massachusetts, USA.
[3]Center for Atmospheric Sciences, University of California, Berkeley, California, USA.
[4]Atmospheric Chemistry Division, National Center for Atmospheric Research, Boulder, Colorado, USA.
[5]Now at Department of Soil, Water and Climate, University of Minnesota, St. Paul, Minnesota, USA.
[6]Now at Department of Atmospheric Science, Colorado State University, Fort Collins, Colorado, USA.

0148-0227/08/2007JD008950

from North America and interpret it on the basis of the underlying vegetation.

[3] Isoprene is produced enzymatically in the chloroplasts of many plants, and escapes to the atmosphere via leaf stomata [*Sharkey and Yeh*, 2001]. Emissions depend strongly on light and temperature, as well as on other factors including plant phenology [*Grinspoon et al.*, 1991; *Monson et al.*, 1994; *Fuentes et al.*, 1995; *Pétron et al.*, 2001], soil moisture [*Sharkey and Loreto*, 1993; *Fang et al.*, 1996], atmospheric composition [*Rosenstiel et al.*, 2003], and nutrient availability [*Harley et al.*, 1994; *Litvak et al.*, 1996]. Emission rates vary widely between plant species, and even between species of the same genus. Broadleaf trees and shrubs are thought to be the most prolific isoprene emitters [*Guenther et al.*, 2006], and carbon emitted as isoprene can then reach several percent of photosynthetic uptake [*Lerdau and Throop*, 1999]. It is not certain why plants emit isoprene, though it may serve to relieve heat stress [*Sharkey and Singsaas*, 1995], serve as an antioxidant [*Stokes et al.*, 1998], or operate as a metabolic safety valve [*Rosenstiel et al.*, 2004].

[4] The first estimates of global biogenic VOC emissions applied simple scaling arguments to the limited data then available, arriving at total emissions of 175–450 Tg a^{-1} [*Went*, 1960; *Rasmussen and Went*, 1965]. As more laboratory and field studies were carried out, inventories were constructed which mapped biogenic VOC emissions according to broad vegetation classes, accounting for the effect of temperature on emission rates [*Zimmerman*, 1979; *Lamb et al.*, 1987; *Rasmussen and Khalil*, 1988; *Turner et al.*, 1991; *Müller*, 1992]. Estimates of global isoprene emissions in these studies ranged from 250–450 Tg a^{-1}, comparable to the earlier estimates of total biogenic VOC emissions. Subsequent inventories improved the discrimination between vegetation classes and accounted for additional factors such as diurnal light and temperature changes, light attenuation through the plant canopy, leaf area, leaf age, and soil moisture [*Lamb et al.*, 1993; *Geron et al.*, 1994; *Guenther et al.*, 1995, 1999, 2006; *Pierce et al.*, 1998]. Recent bottom-up emission inventories estimate global isoprene emissions at 500–750 Tg a^{-1} [*Guenther et al.*, 1995, 2006]. However, simulations with chemical transport models (CTMs) have found that these higher emission rates yield excessive levels of CO, O_3, and isoprene itself when compared to observations [*Houweling et al.*, 1998; *Poisson et al.*, 2000; *Bey et al.*, 2001]. The Intergovernmental Panel on Climate Change (IPCC) Working Group on Atmospheric Chemistry and Greenhouse Gases [*Ehhalt and Prather*, 2001] recommends a global isoprene flux of only 220 Tg a^{-1}. On a regional scale, uncertainties are even larger [*Guenther et al.*, 2006]. Given the importance of isoprene in tropospheric chemistry, there is a need to test and improve the bottom-up emission estimates.

[5] Formaldehyde measurements from space offer the capability to map isoprene emissions on a global, continuous basis, and provide a top-down test of the bottom-up inventories. Since isoprene has an atmospheric lifetime of less than 1 hour and yields HCHO as first-generation product in the presence of NO, HCHO column measurements from space provide a proxy for isoprene emissions [*Palmer et al.*, 2003]. *Millet et al.* [2006] demonstrated the validity of this approach by using combined HCHO and isoprene aircraft measurements over North America. They estimated an overall uncertainty of 40% in inferring isoprene emissions from HCHO satellite measurements, with clouds the largest source of error.

[6] Previous work to interpret HCHO column measurements from space as constraints on isoprene emissions used data from the Global Ozone Monitoring Instrument (GOME) aboard the ERS-2 satellite launched in 1995 [*Abbot et al.*, 2003; *Palmer et al.*, 2003, 2006; *Shim et al.*, 2005]. These revealed general consistency with prior understanding of the seasonal and interannual variability of isoprene emission [*Abbot et al.*, 2003; *Palmer et al.*, 2003, 2006], but also large regional discrepancies [*Palmer et al.*, 2003; *Shim et al.*, 2005]. GOME had a coarse footprint of 40×320 km^2, making it subject to large cloud errors, and required 3 days to achieve global coverage; the ability to interpret the data in terms of testing emission models was thus limited [*Palmer et al.*, 2006]. HCHO columns have also been reported from the SCIAMACHY sensor aboard the Envisat satellite launched in 2002 [*Wittrock et al.*, 2006], but at a resolution which is only marginally better (60×120 km^2) and with global coverage only every six days.

[7] OMI, launched in 2004 with a nadir footprint of only 13×24 km^2 and daily global coverage [*Levelt et al.*, 2006], affords unprecedented top-down constraints on the spatial distribution of isoprene emissions. The higher spatial resolution also reduces data contamination by clouds [*Millet et al.*, 2006; *Krijger et al.*, 2007]. Here we apply HCHO column measurements from OMI to develop spatial constraints on isoprene emissions from North America that are of much higher quality than achievable from GOME. We exploit the higher quality of the OMI data to test current isoprene emission models in terms of isoprene emission capacity from plant functional types.

2. OMI HCHO Observations and Comparison to GOME

2.1. OMI Observations

[8] OMI was launched on-board EOS Aura in July 2004 into a sun-synchronous orbit with an equator crossing time of 13:38 (ascending node). OMI is a UV/Vis CCD spectrometer covering the spectral range 270–500 nm with a resolution of 0.45–1.0 nm full width at half maximum. A cross-track swath of 2600 km, containing 60 pixels ranging from 13×24 km^2 at nadir to 26×135 km^2 at the swath edges, provides daily global coverage. Here we use an optimized fitting window (324–348 nm) for the HCHO retrieval, selected to correct a low bias, excessive across-track striping, and land-sea correlation in the current publicly released data product (Version 1.0.0). Below we evaluate the consistency of this updated OMI product with data from GOME in previous years. The retrieval determines the HCHO abundance along the viewing path ("slant column") by non-linear least squares fitting of measured radiances and irradiances, including molecular absorption cross sections, correction for Ring effect, albedo, and a low-order closure polynomial [*Chance*, 2002]. The retrieval includes solar and radiance wavelength calibrations and undersampling correction [*Chance et al.*, 2005] in addition to the fitting itself. We use a composite solar spectrum

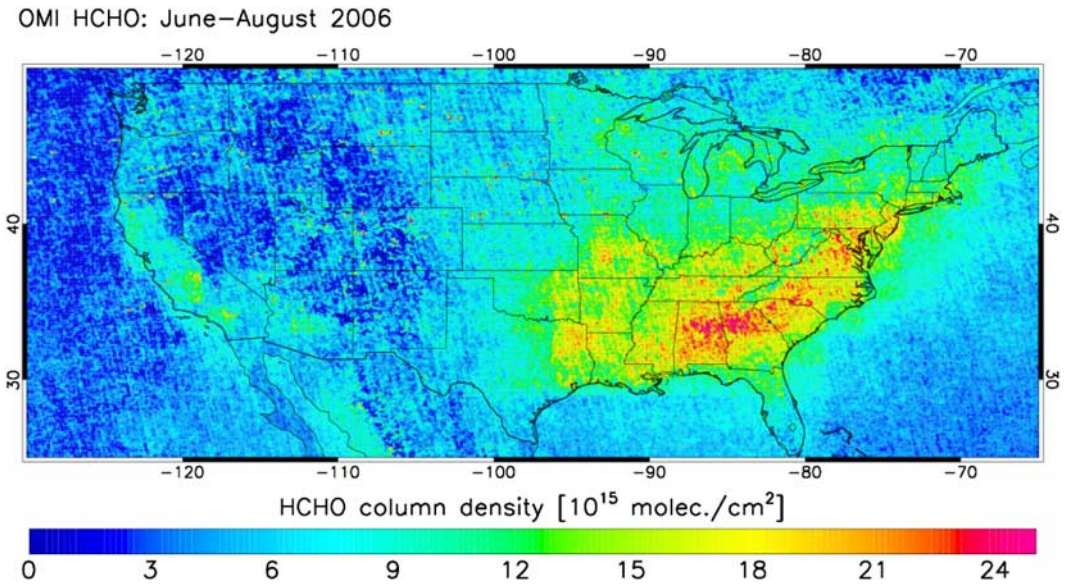

Figure 1. Mean OMI HCHO columns for June–August 2006 mapped on a 0.1° × 0.1° grid.

(derived from a principal component analysis of several hundred OMI irradiance measurements) in place of the individual irradiances in order to reduce uncertainties introduced by dark current in the detector signal.

[9] While previous analyses with GOME imply an HCHO fitting uncertainty of 4×10^{15} molecules cm^{-2} [*Chance*, 2002], those for individual OMI measurements are higher ($\sim 2 \times 10^{16}$ molecules cm^{-2} over North America). However, this uncertainty is strongly reduced by temporal averaging, due to OMI's improved (100–200×) sampling statistics resulting from the smaller footprint and better temporal coverage. For a 3-month average at 1° × 1° (as will be used here), each grid square contains on average 870 cloud-free OMI observations, so that the random error is small (average standard error <10%).

[10] Cloud information for each OMI scene (version 1.0.1.1; http://daac.gsfc.nasa.gov/) is obtained from the O_2-O_2 absorption band around 477 nm, which yields the slant column of the O_2-O_2 collision complex and the continuum reflectance (i.e., the reflectance in the absence of the O_2-O_2 absorption). The cloud pressure and effective cloud fraction are then derived assuming a Lambertian reflector with an albedo of 0.8 [*Acarreta et al.*, 2004].

[11] The ratio of the slant column to the actual vertical column, termed the air mass factor (AMF), is a function of the viewing geometry, surface reflectance and atmospheric scattering (air molecules, aerosols, clouds), and the vertical distribution of HCHO relative to that of the atmospheric scatterers [*Perliski and Solomon*, 1993; *Marquard et al.*, 2000; *Palmer et al.*, 2001; *Boersma et al.*, 2004; *Millet et al.*, 2006]. Here we use the GEOS-Chem CTM (described below) to specify the shape of the HCHO vertical profile at the time and location of the satellite overpass. Surface UV albedos (340–380 nm) are from a TOMS climatological database [*Herman and Celarier*, 1997]. In our previous work we showed that this approach to calculating the AMF, combined with fitting errors, gives an overall 1σ error in HCHO column retrievals of 25–27% for cloud fraction <0.2 [*Millet et al.*, 2006].

[12] Scattering weights have been computed with the Doubling Adding KNMI (DAK) radiative transfer model [*Stammes*, 2001] at a wavelength of 348.0 nm and stored in a lookup table as a function of atmospheric pressure level, sun-satellite geometry, surface albedo, and surface pressure. Multiple scattering and the sphericity of the Earth's atmosphere are accounted for in the radiative transfer calculations. Clouds are represented by Lambertian surfaces with an albedo of 0.8, as recommended by *Koelemeijer and Stammes* [1999], and consistent with the O_2-O_2 cloud algorithm used here. We exclude data with cloud fraction >0.2 from our analysis. Statistical outliers (|slant column| > 1.0×10^{18} molecules cm^{-2}) are removed prior to gridding, as are low sun retrievals (solar zenith angle >84°), and data points where the HCHO slant column is negative within 1σ fitting uncertainty. OMI HCHO exhibits a small, latitude-dependent bias which we correct by adjusting to the HCHO columns simulated by the GEOS-Chem CTM over the clean East Pacific. The mean correction is 1×10^{15} molecules cm^{-2} for the domain of interest here (25°–50°N), well within the HCHO fitting uncertainty.

[13] Figure 1 shows the average OMI HCHO vertical columns (gridded to 0.1° × 0.1°) over North America for June-August 2006. We show here data smoothed by means of a cross-track filter [*Kurosu*, 2007] to remove the striping exhibited by OMI (due to dark current in the radiance and irradiance spectra) at this fine resolution. The smoothing does not significantly change the across-track column averages (and becomes unnecessary at the 1° × 1° resolution used for subsequent analyses below). The most prominent feature in Figure 1 is the elevated HCHO over the U.S. Southeast, extending from eastern Texas to the mid-Atlantic coast. HCHO columns are generally low over the western United States, with the exception of some minor enhancements over California. Below in section 3.2 we examine these measured HCHO columns in the context of the spatial distribution of biogenic and anthropogenic precursor emissions.

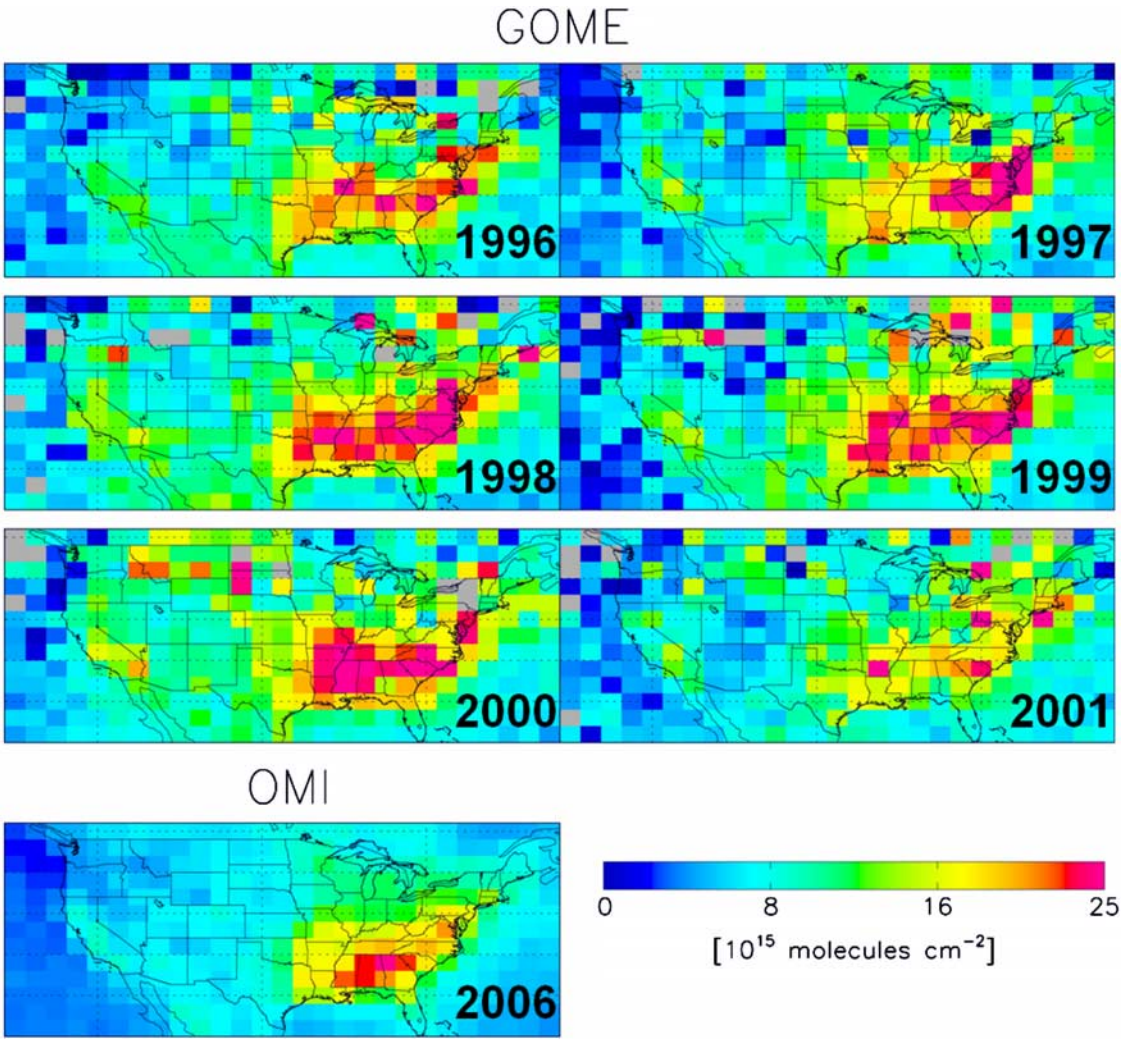

Figure 2. Mean June–August HCHO columns from GOME (1996–2001) and OMI (2006) mapped on a 2° × 2.5° grid.

2.2. Comparison to GOME

[14] Previous analyses of HCHO column data from space relied primarily on GOME data from 1996 to 2001 [*Abbot et al.*, 2003; *Palmer et al.*, 2003, 2006; *Meyer-Arnek et al.*, 2005; *Shim et al.*, 2005; *Fu et al.*, 2007]. GOME data quality degraded considerably after 2001. OMI was launched in 2004, which precludes a direct large-scale comparison of the two instruments. Nevertheless, we can evaluate their consistency by comparing HCHO column measurements from the same season in different years.

[15] Figure 2 shows June-August HCHO columns from GOME (1996–2001) and OMI (2006) mapped on a 2° × 2.5° (latitude × longitude) grid over our North American domain (65–130°W, 25–50°N). We use here a cloud fraction threshold of 0.4 (versus 0.2 elsewhere) for both GOME and OMI in order to obtain sufficient data in the case of GOME. For both retrievals we use absorption cross sections from *Cantrell et al.* [1990]. The 2° × 2.5° grid is that used in the GEOS-Chem CTM for further analysis later on in this paper, but it is also helpful here to accommodate the coarse resolution of GOME (40 × 320 km^2). Both OMI and GOME show an HCHO maximum over the U.S. Southeast, though the GOME values are higher and exhibit more retrieval noise. Table 1 shows the OMI vs. GOME regression statistics for correlation of the mean June–August spatial distributions. The coefficient of determination R^2 ranges from 0.29 to 0.61, with the worst correlation in the

Table 1. OMI Versus GOME Comparison Statistics Over North America[a]

Year	R^2	Slope[b]	Intercept[b] [10^{15} molecules cm^{-2}]
1996	0.57	0.83 ± 0.04	−0.02 ± 0.35
1997	0.60	0.84 ± 0.04	−0.17 ± 0.33
1998	0.58	0.75 ± 0.03	−0.41 ± 0.37
1999	0.42	0.70 ± 0.04	0.68 ± 0.37
2000	0.42	0.78 ± 0.04	−0.98 ± 0.45
2001	0.29	0.92 ± 0.06	−0.56 ± 0.50

[a]OMI measurements for June–August 2006 are compared to GOME measurements for June–August of individual years 1996–2001. Correlation statistics are shown for the spatial variability of the June–August mean values mapped on a 2° × 2.5° grid.

[b]Coefficients determined using reduced major axis regression. Stated uncertainties represent one standard error calculated using jackknife resampling.

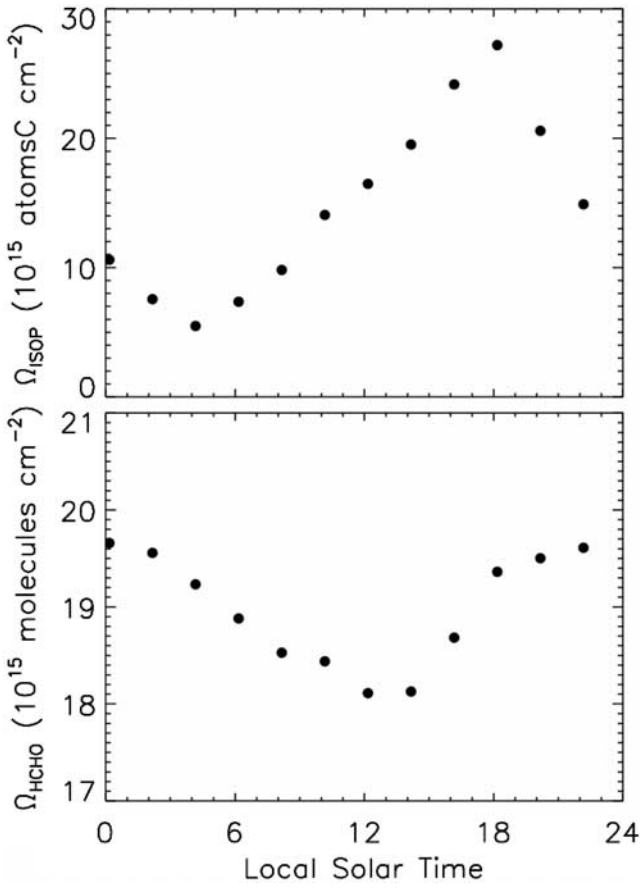

Figure 3. Mean diurnal cycle in GEOS-Chem simulated isoprene (top) and HCHO (bottom) columns over the U.S. Southeast (32–38°N, 80–95°W) during June–August.

later years of the degrading GOME record. Other factors likely reducing the GOME-OMI correlation are interannual variability and poor sampling statistics for GOME (average 22–36 observations per grid cell; range 0–87) compared to OMI (average 4400 observations per grid cell; range 2000–6500). The intercepts, ranging from -0.98–0.68×10^{15} molecules cm^{-2}, are small relative to the OMI and GOME detection limits. The OMI versus GOME slopes are all less than one (ranging from 0.70 ± 0.04 to 0.92 ± 0.06), indicating a systematic offset between the two instruments.

[16] The GOME overpass time is 10:30, three hours earlier than OMI, and HCHO surface concentrations are typically highest in the mid-afternoon [e.g., *Sumner et al.*, 2001]. However, Figure 3 shows that GEOS-Chem HCHO columns over the U.S. Southeast vary by only 2% between late morning and early afternoon. This weak diurnal variation results from HCHO having both a daytime source and a daytime sink, combined with the isoprene column peaking in the mid to late afternoon. We conclude that the difference in local overpass time is not a significant factor in the GOME-OMI offset.

[17] Previous analysis of the GOME record for 1996–2001 identified significant interannual variability over the United States that could be largely explained by temperature [*Palmer et al.*, 2006]. Figure 4 shows monthly mean HCHO columns over the U.S. Southeast (32–38°N, 80–95°W) from both GOME and OMI, plotted as a function of the surface air temperature as in the work of *Palmer et al.* [2006]. The exponential fit to the GOME data ($R^2 = 0.73$) describes the sensitivity of isoprene emission to temperature following *Guenther et al.* [1999]. We see that the relationship between HCHO columns and temperature is consistent between the two instruments. However, the OMI measurements (in red) fall 2–14% below the curve defined by the ensemble of the GOME data. *Millet et al.* [2006] showed that HCHO retrieval bias increases with cloud fraction, from 6% at a cloud fraction of 0.2 to 14% at a cloud fraction of 0.4. Thus the observed OMI-GOME difference is consistent with what we expect from systematic error in the retrievals.

[18] Different cloud algorithms used in the two retrievals could be contributing to the 2-14% discrepancy. Cloud fraction and pressure are derived from O_2 *A* band spectra in the case of GOME [*Kurosu et al.*, 1999] and from O_2-O_2 spectra in the case of OMI (which does not detect the O_2 *A* band at 760 nm). *Boersma et al.* [2007] compared O_2 *A* band and O_2-O_2 based cloud products, and found that while the average cloud fractions agreed to ~1%, the O_2-O_2 cloud pressures were higher by a mean of 60 hPa. The latter will result in a lower computed absorber column for O_2-O_2 versus O_2 *A* band clouds, particularly in the case of low clouds [*Boersma et al.*, 2004].

3. Models for OMI Data Interpretation

3.1. MEGAN Bottom-up Model of Isoprene Emissions

[19] We use the Model of Emission of Gases and Aerosols from Nature (MEGAN) [*Guenther et al.*, 2006] as the best process-based estimate of isoprene emissions for North America. MEGAN was developed to replace the earlier Global Emission Inventory Activity (GEIA) model [*Guenther et al.*, 1995] as well as the regional Biogenic Emission

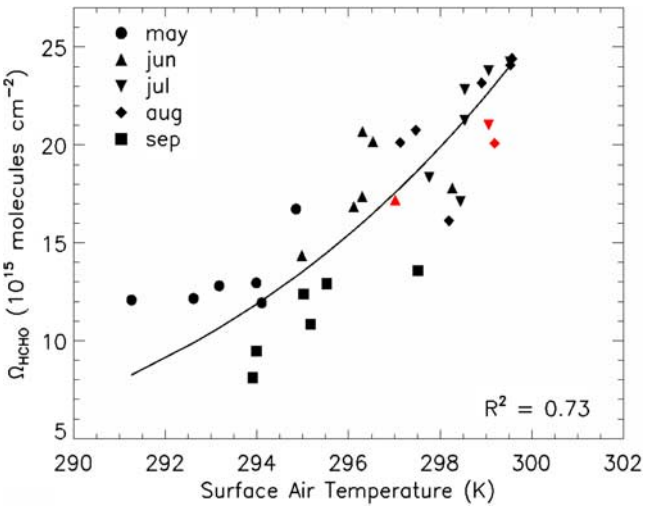

Figure 4. Monthly mean HCHO vertical columns over the U.S. Southeast (32–38°N, 80–95°W) from GOME (1996–2001; black symbols) and OMI (2006; red symbols), as a function of the surface air temperature. The black line shows a fit of the GOME data to an exponential describing the temperature dependence of isoprene emission [*Guenther et al*, 1999, equation (5a)]. Figure adapted from *Palmer et al.* [2006].

Inventory System (BEIS) models for the United States [*Pierce et al.*, 1998], by including updated information on base emissions and environmental dependences. Emissions are computed as a function of solar irradiance, temperature, leaf age and vegetation-specific emission factors (EFs) for six plant functional types (PFTs): broadleaf trees, shrubs, fineleaf evergreen trees, fineleaf deciduous trees, crops, and grass + other. Isoprene emission E for a given area (e.g., model grid square) is given by

$$E = \gamma \sum_{i=1}^{6} \varepsilon_i \chi_i, \quad (1)$$

where the sum is over all PFTs with fractional areal coverage χ_i and canopy emission factor ε_i under standard conditions of light, temperature, leaf area index (LAI) and leaf age; and γ is an activity factor accounting for emission changes due to local variability in those parameters (equation (2)). The EFs for a given PFT vary geographically according to the local taxonomic makeup of the PFT. Species-level PFT composition is obtained from quantitative ground surveys where available, and estimated from the terrestrial ecoregion database developed by *Olson et al.* [2001] elsewhere. The overall activity factor γ is the product of a set of non-dimensional activity factors each equal to one at standard conditions

$$\gamma = \gamma_T \gamma_{PAR} \gamma_{LAI} \gamma_{age}. \quad (2)$$

[20] The temperature activity factor γ_T is a function of the current temperature and the mean local temperature over the past 15 days, while the light activity factor γ_{PAR} is calculated as an integral over the canopy depth to account for light attenuation and the effect of direct and diffuse light on sunlit and shaded leaves [*Guenther et al.*, 1999]. The activity factors γ_{LAI} and γ_{age} account for emission changes due to seasonal variation in local leaf area index and leaf age [*Guenther et al.*, 2006]. The MEGAN algorithm to account for isoprene emission variations driven by soil moisture was not implemented for this study. The soil moisture option results in decreased isoprene emissions during drought and is not likely to have a significant impact in areas of major isoprene emission in North America.

[21] We drive MEGAN with assimilated meteorology (surface air temperature, direct and diffuse photosynthetically active radiation) at $2^\circ \times 2.5^\circ$ horizontal resolution and 3 hour temporal resolution from the NASA Goddard Earth Observing System (GEOS-4), using monthly LAI derived from the Advanced Very High Resolution Radiometer (AVHRR) Pathfinder Normalized Difference Vegetation Index data set [*Myneni et al.*, 1997].

[22] The isoprene emission calculated with MEGAN depends on the choice of vegetation database used to assign fractional coverage for each PFT within a grid square. Here we use two different databases to examine the sensitivity to that choice. The first, MEGAN Driving Variables Database version 2.0 (MDVD2), is the standard case for the analysis described by *Guenther et al.* [2006]. The MDVD2 PFT fractions integrate the percentage vegetation coverage and type (woody vs. herbaceous) at 500 m resolution from MODIS [*Hansen et al.*, 2003] with leaf longevity (evergreen vs. deciduous) and leaf type (broadleaf versus needleleaf) from the 1 km AVHRR-derived University of Maryland tree cover data set [*DeFries et al.*, 2000]. Relative abundance of the non-tree PFTs is determined from ground survey information where available and the *Olson et al.* [2001] ecoregion database elsewhere. The AVHRR-based broadleaf and needleleaf PFT fractions in the United States are adjusted using ground survey information compiled by *Kinnee et al.* [1997]. The second vegetation database is from the Community Land Model (CLM) [*Oleson et al.*, 2004]. CLM obtains percentage tree cover, leaf type, and leaf longevity from AVHRR [*DeFries et al.*, 2000], and understory and herbaceous PFT distributions from the IGBP DISCover land cover data set [*Loveland et al.*, 2000] (also derived from AVHRR). We lump the 16 CLM vegetation types into categories corresponding to the six MEGAN PFTs.

[23] Figure 5 shows the percent distribution of the 6 PFTs according to the MDVD2 and CLM vegetation databases, along with the associated isoprene EFs. Broadleaf trees are the largest isoprene emitters and are concentrated in the eastern United States. Shrubs also have a high EF and are more abundant in the arid West. However, because of their lower leaf area, the resulting isoprene emissions are lower than those from broadleaf trees. The other four PFTs are only minor isoprene sources according to MEGAN.

[24] There are significant differences between MDVD2 and CLM in the estimated distributions of the PFTs. MDVD2 has more broadleaf trees in the Deep South and along the Southern to Mid-Atlantic coast, where CLM assigns more of the vegetation coverage to fineleaf evergreen trees and grasses. CLM has more broadleaf trees in the U.S. Northeast and Midwest, where MDVD2 tends to put more crops and shrubs. Both MDVD2 and CLM have the highest density of shrubs in the West, but the difference is more dramatic in CLM, with no shrubs in the East.

[25] Figure 6 shows MEGAN isoprene emissions computed using MDVD2 and CLM. *Guenther et al.* [2006] compared global annual average isoprene emissions using these two databases and found CLM emissions to be 7% lower. Here, focusing on North America for June-August 2006, we find that both MDVD2 and CLM-driven emissions are highest in the Southeast and Mid-Atlantic regions, but there are large differences. The total North American emission for the domain of Figure 6 is 18% higher in MDVD2 (14.6 TgC) than in CLM (12.2 TgC). Regional differences often exceed a factor of 2. The Southeast emission maximum in CLM is focused in the Ozark Plateau (Arkansas/Missouri) and the Upper South, while with MDVD2 the greater regional abundance of broadleaf trees leads to elevated emissions extending through the Deep South to the Gulf coast. CLM emissions are higher than MDVD2 in the Upper Midwest, again because of higher estimated broadleaf tree coverage. Below we will use HCHO column measurements from OMI to test these different results.

3.2. GEOS-Chem Chemical Transport Model

[26] We use the GEOS-Chem global 3D CTM [*Bey et al.*, 2001; *Millet et al.*, 2006; *Palmer et al.*, 2006] to simulate the HCHO vertical distribution needed for the AMF calculation in the OMI retrieval, and to quantify the relationship

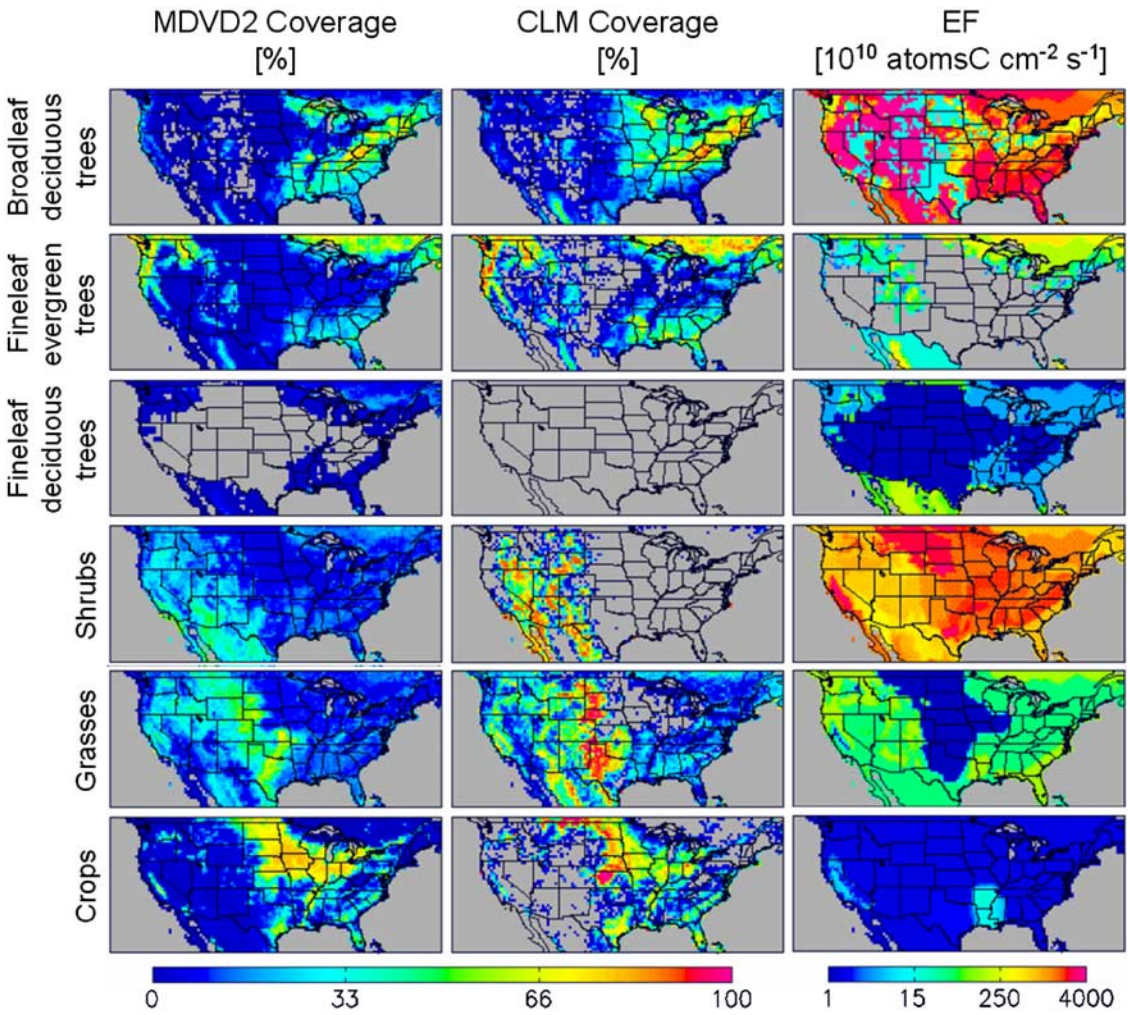

Figure 5. Fractional coverage of the six plant functional types (PFTs) in the MDVD2 and CLM databases, and isoprene emission factors (EFs) for each PFT. Note that the emission factors are plotted on a logarithmic scale. Zero values are plotted in grey. Isoprene emissions are computed as the product of PFT coverage and EFs, scaled to local environmental conditions (equation (1)).

between HCHO columns and isoprene emission. GEOS-Chem (version 7.04, http://www-as.harvard.edu/chemistry/trop/geos/index.html) uses GEOS-4 assimilated meteorological data including winds, convective mass fluxes, mixing depths, temperature, precipitation, and surface properties. The data have 6-h temporal resolution (3-h for surface variables and mixing depths), $1^\circ \times 1.25^\circ$ horizontal resolution, and 55 vertical layers. We degrade the horizontal resolution to $2^\circ \times 2.5^\circ$ for input to GEOS-Chem. Results are presented here for June through August 2006, and follow a one year spinup.

[27] The model includes detailed ozone-NO_x-VOC chemistry coupled to aerosols. HCHO is produced from oxidation of VOCs, and removed by reaction with OH and photolysis on a timescale of a few hours (there is also a minor deposition sink). Biogenic emissions of isoprene, monoterpenes, and 2-methyl-3-buten-2-ol are calculated using the MEGAN inventory, and those of acetone and methanol are based on *Jacob et al.* [2002] and *Jacob et al.* [2005], respectively. Biogenic alkene emissions are scaled to 10% of isoprene based on work by *Goldstein et al.* [1996, 1998]. Anthropogenic emissions are from the EPA NEI 1999 v.1 inventory [*EPA*, 2003], except that anthropogenic emissions of ethane and propane are based on *Wang et al.* [1998] for reasons discussed by *Hudman et al.* [2007], and NO_x emissions from power plants and industry have been decreased by 50% following *Hudman et al.* [2007] and *Frost et al.* [2006]. *Millet et al.* [2006] compared HCHO mixing ratios simulated using GEOS-Chem with observations over North America and the North Atlantic from the NASA INTEX-A aircraft experiment. Both the HCHO vertical distribution and column amount were well simulated, with no apparent biases.

[28] Figure 7 shows the modeled total anthropogenic and biogenic VOC emissions for June-August, 2006. Biogenic emissions (MDVD2) are 7 times greater than anthropogenic VOC emissions over North America, with the highest anthropogenic contribution in the Northeast and industrialized Midwest. According to MEGAN, isoprene accounts for

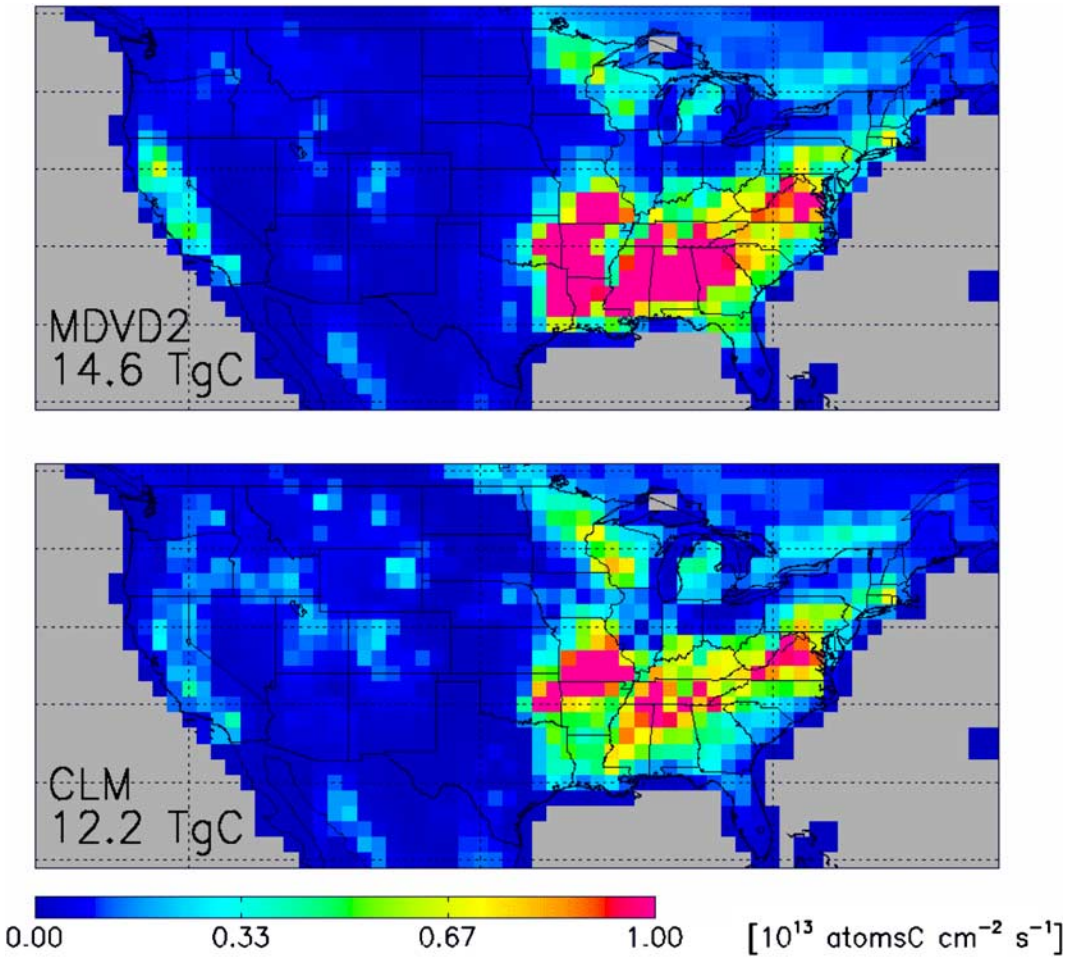

Figure 6. Mean MEGAN isoprene emissions (1° × 1°) at 12:00-15:00 local time for June-August 2006 computed using MDVD2 and CLM land cover. Numbers inset give total (24-h) isoprene emissions for the same time period. Note that the color scale saturates; the maximum plotted values are 2.2×10^{13} (MDVD2) and 1.9×10^{13} (CLM) atomsC cm^{-2} s^{-1}.

70% of the total biogenic VOC source over our North American domain (Figures 6 and 7).

[29] Figure 8 shows HCHO columns simulated by GEOS-Chem using MDVD2 and CLM land cover. The simulated spatial variability in the HCHO column maps that of isoprene emission (Figure 6) and has little influence from anthropogenic VOC emissions. The dominance of isoprene in determining HCHO column variability over the eastern United States was inferred previously from aircraft measurements [*Millet et al.*, 2006]. Here we find that large metropolitan areas with the highest anthropogenic VOC emissions (such as New York, Chicago, and Los Angeles), are not associated with strong HCHO column enhancements in the OMI data, even at 0.1° × 0.1° resolution (Figure 1). A minor HCHO enhancement is apparent over Houston in Figure 1, likely due to oxidation of olefins emitted in large quantities from the local petrochemical industry [*Jobson et al.*, 2004]. HCHO concentrations measured below 1500 m over the Houston ship channel (where the petrochemical industry is concentrated) during the TexAQS aircraft campaign in August-September 2000 averaged 4–8 ppb [*Martin et al.*, 2004]. A mixing ratio of 6 ppb below 1500 m and 0.3 ppb above corresponds to a total column amount of approximately 2×10^{16} molecules cm^{-2}, which is consistent with the enhancement seen by OMI over that region (Figure 1). *Martin et al.* [2004] found that even in the vicinity of Houston (with its extremely high petrochemical VOC emissions), the highest HCHO columns (derived from aircraft measurements) were found over isoprene-emitting hardwood forests north and east of the city.

[30] Overall, Figure 1 shows that anthropogenic VOCs are a negligible source of variability in column HCHO over the entire United States. In contrast, *Fu et al.* [2007] observed significant HCHO enhancements (measured by GOME) over Chinese cities, consistent with urban VOC emission inventories (to within 25%). Current bottom-up emission inventories indicate that U.S. on-road VOC emissions (the dominant urban source) have declined by 70% or more since the 1970s [*Parrish*, 2006; *EPA*, 2007]. The OMI HCHO data present a consistent picture, showing that after 3 decades of regulation, anthropogenic reactive VOC emissions from the U.S. are small compared to the large biogenic source.

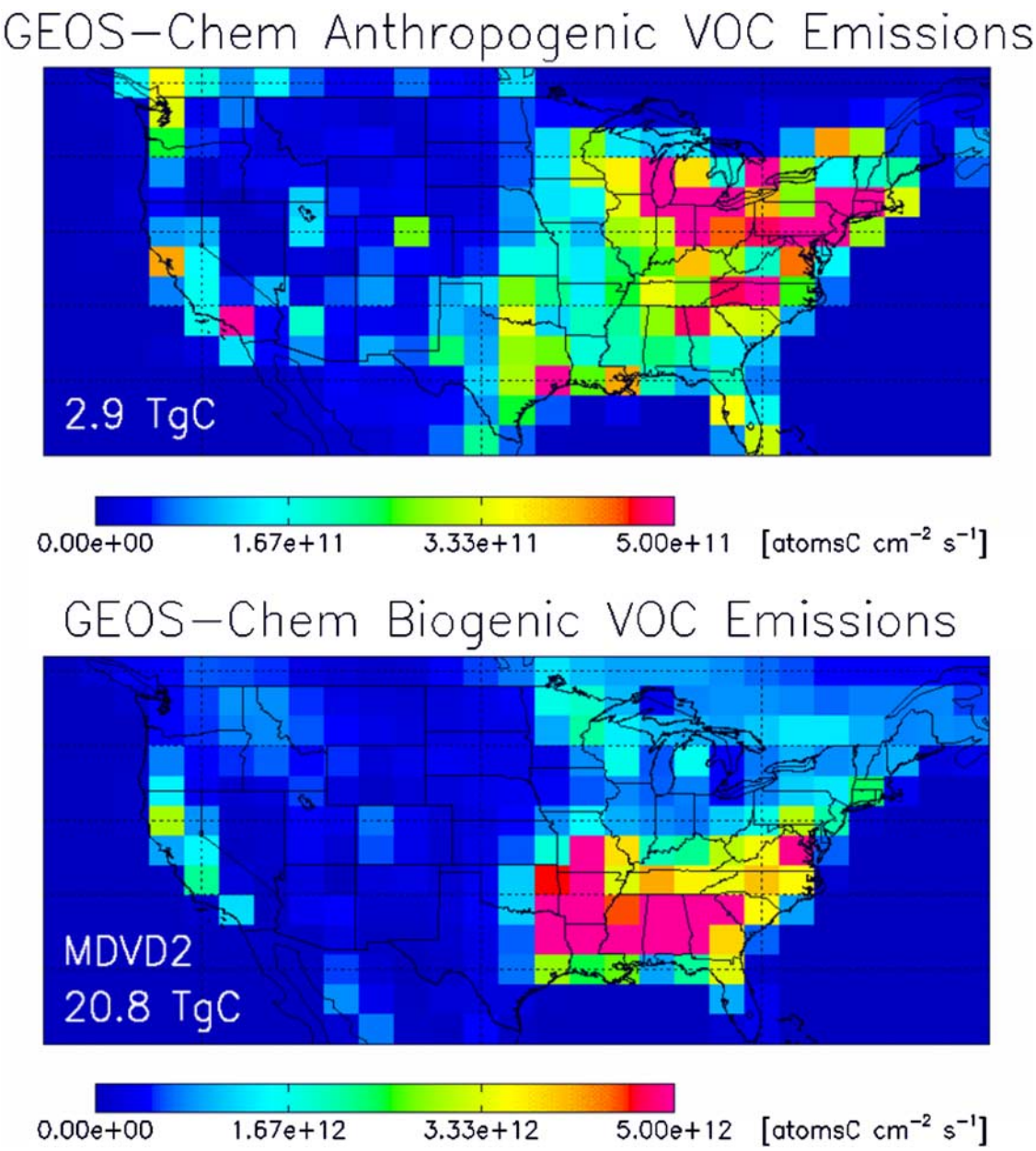

Figure 7. Total (24-h average) anthropogenic and biogenic VOC emissions for June-August 2006 in GEOS-Chem (see text for details). Note the factor of 10 scale difference between the two panels. The color scales saturate; the maximum plotted values are 1.4×10^{12} (anthropogenic) and 8.0×10^{12} (biogenic) atomsC cm^{-2} s^{-1}.

[31] Figure 9 shows a scatterplot of OMI HCHO columns vs. those simulated by GEOS-Chem using MEGAN driven by the MDVD2 and CLM land cover databases. In both cases the modeled and measured HCHO columns are highly correlated (R^2 = 0.92 and 0.85), but the modeled HCHO columns are biased high at the upper end of the distribution; this corresponds mainly to the U.S. Southeast. The problem is more pronounced with the MDVD2 database. The high correlation is in part a result of smoothing over the 2° × 2.5° model grid; we will see below that the correlation breaks down at higher resolution. Previous work has found a lower correlation (R^2 = 0.7) between GOME HCHO columns over North America in summer and those simulated by GEOS-Chem driven by the GEIA biogenic emission inventory [*Shim et al.*, 2005; *Palmer et al.*, 2006]. The improvement shown here is likely due to a more accurate treatment of land cover and vegetation-specific emission factors in MEGAN vs. GEIA [*Guenther et al.*, 1995, 2006], as well as to the improved counting statistics for OMI vs. GOME.

4. Relating HCHO Columns to Isoprene Emission

[32] In the absence of horizontal wind, the HCHO column Ω_{HCHO} would be related to the emission rates of VOC

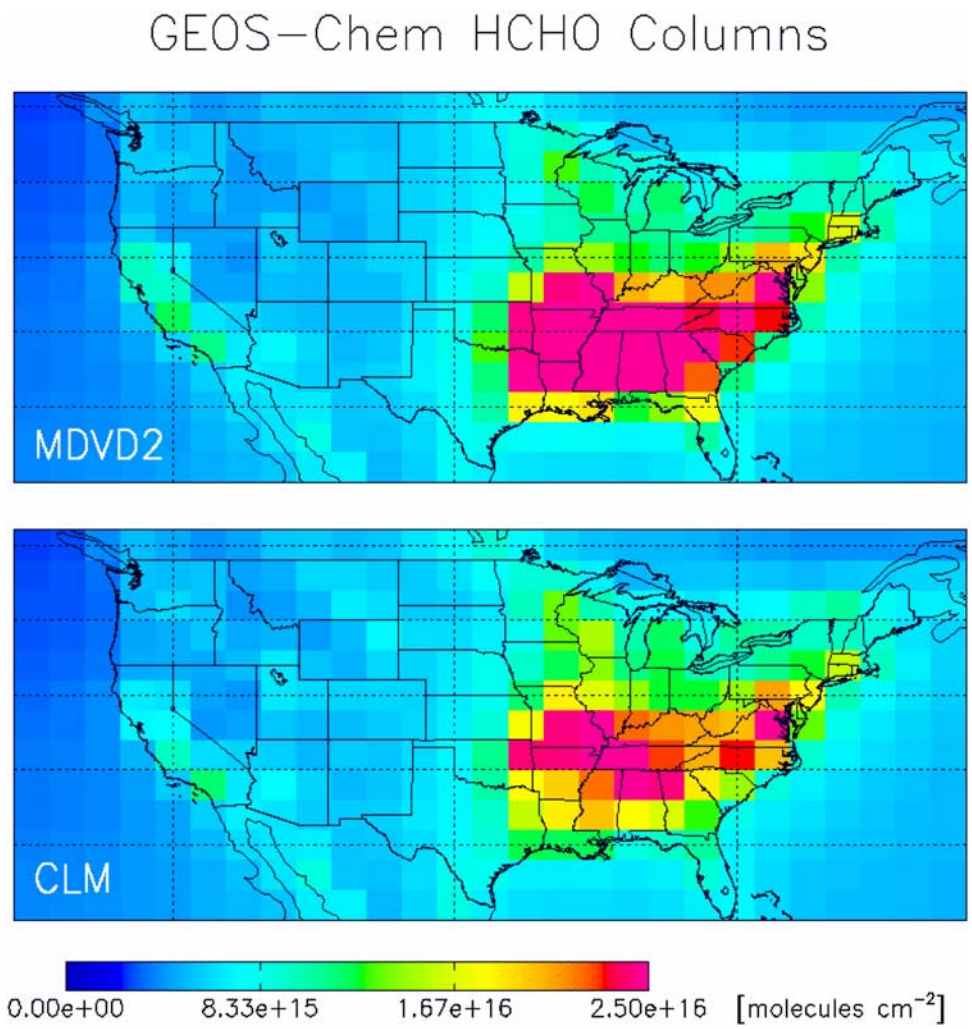

Figure 8. GEOS-Chem HCHO columns at 12:00–15:00 local time (June-August 2006) simulated using the MEGAN biogenic emission inventory driven by MDVD2 and CLM land cover. The color scales saturate; the maximum plotted values are 3.5×10^{16} (MDVD2) and 2.7×10^{16} (CLM) molecules cm^{-2}.

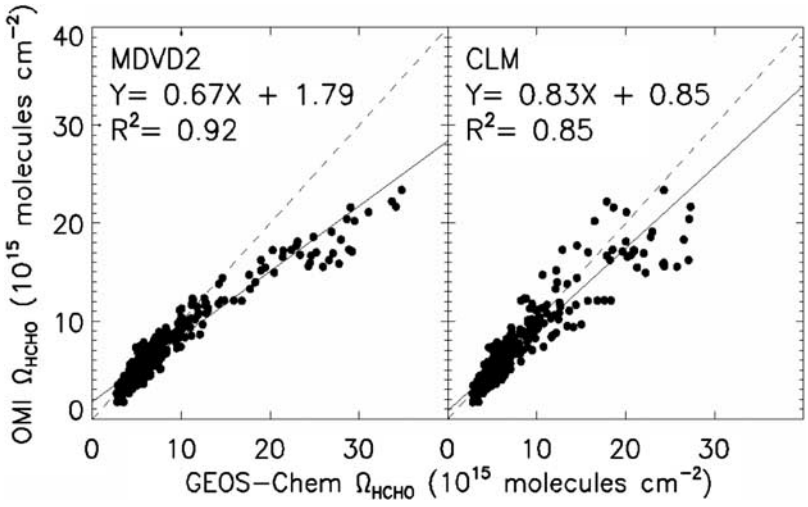

Figure 9. OMI vs. GEOS-Chem HCHO columns (12:00–15:00 local time) over North America (65–130°W, 25–50°N). Each point represents the mean June-August 2006 value for a 2° × 2.5° model grid square. GEOS-Chem uses the MEGAN inventory with the MDVD2 (left) and CLM (right) vegetation databases.

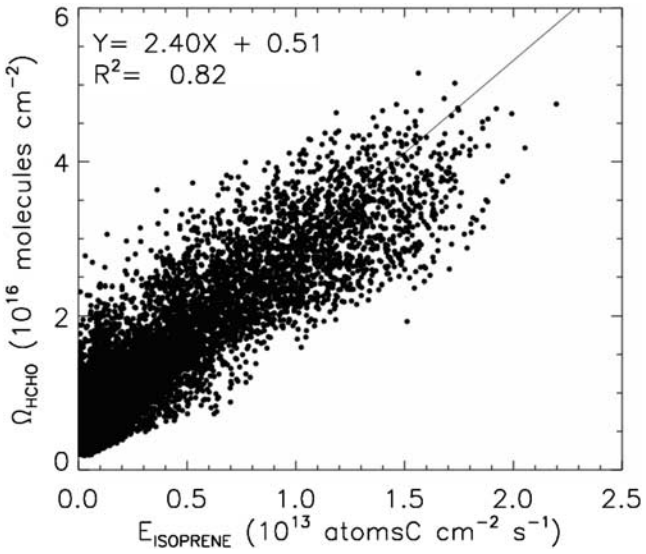

Figure 10. GEOS-Chem relationship between HCHO column and isoprene emission at 12:00–15:00 local time over North America (65–130°W, 25–50°N) for June-August 2006, taking the whole domain as a single statistical population. Each point represents one day (12:00–15:00 average) for one model grid square. The reduced major axis regression line is also shown with regression statistics given inset.

precursors by

$$\Omega_{\mathrm{HCHO}} = \frac{1}{k_{\mathrm{HCHO}}} \sum_i Y_i E_i, \tag{3}$$

where Y_i is the HCHO yield from the oxidation of precursor i with emission rate E_i, and k_{HCHO} is the column-integrated HCHO loss rate constant. Direct (primary) emissions of HCHO from biogenic [*Kesselmeier and Staudt*, 1999] and anthropogenic [*EPA*, 2003] sources in North America are minor relative to secondary production, so that we can neglect them here. Horizontal wind smears this relationship according to the lifetime of the parent VOC with respect to HCHO production and that of HCHO itself. *Palmer et al.* [2003] estimated the smearing length scale induced by the time lag between isoprene emission and HCHO production, and the HCHO lifetime, at ~50 km under typical conditions, so that on a 1° × 1° grid (as used here) the smearing can be neglected. As shown by *Palmer et al.* [2003, 2006], VOCs other than isoprene generally either have excessive smearing or insufficient emission relative to the HCHO detection limit, so that HCHO column observations from space are highly specific to isoprene. This was confirmed by *Millet et al.* [2006] using concurrent VOC and HCHO aircraft measurements over eastern North America in summer.

[33] *Palmer et al.* [2003] fitted the relationship between isoprene emission and HCHO columns in GEOS-Chem for each U.S. quadrant (defined by longitudinal and latitudinal divides at 100°W and 40°N) to a linear regression

$$\Omega_{\mathrm{HCHO}} = SE_{isop} + B, \tag{4}$$

where the slope S reflects the HCHO yield from isoprene oxidation and the column-integrated HCHO loss rate constant (equation (3)), and the intercept B represents the background HCHO column arising from the oxidation of other VOC precursors. They then used this relationship to infer isoprene emissions from the HCHO columns measured by GOME. The geographical division by U.S. quadrants had no particular justification. We improve here on this work with a more deliberate analysis of the geographical variability of the $\Omega_{\mathrm{HCHO}} - E_{isop}$ relationship. The quality of the correlation is expected to vary with the concentration of NO (affecting the timescale for conversion of isoprene to HCHO; [*Palmer et al.*, 2006]) and with the distribution of isoprene emission upwind; in addition, S is expected to vary with the local photochemical environment. Inasmuch as GEOS-Chem has predictive capability in simulating this variability in S, it should be taken into account when inferring E_{isop} from Ω_{HCHO}. One has to be cautious, however, as model errors in simulating the variability in S will generate spurious variability in the inferred isoprene emissions. We consider here two limiting cases. In the first, we apply a single uniform $\Omega_{\mathrm{HCHO}} - E_{isop}$ relationship, derived from linear regression over the entire North American domain (65–130°W, 25–50°N); spatial variability in the retrieved isoprene emission fluxes is then solely determined by the OMI data. In the second, we use a spatially resolved $\Omega_{\mathrm{HCHO}} - E_{isop}$ relationship for each model grid square; the variability then contains model information related to the photochemical environment and the local pattern of isoprene emission.

[34] Figure 10 shows the simulated $\Omega_{\mathrm{HCHO}} - E_{isop}$ relationship at 12:00–15:00 local time for the entire North American analysis domain (65–130°W, 25–50°N), computed using MDVD2 land cover (using CLM land cover does not significantly change the regression results). The coefficient of determination ($R^2 = 0.82$) implies that 80% of the spatial variability in isoprene emission can be resolved using space-based measurements of the HCHO column. The slope S (2.4×10^3 s) can be compared to a value of 2.1×10^3 s estimated from measurements of HCHO mixing ratio and isoprene flux over a Michigan forest [*Palmer et al.*, 2006], and a value of 2.3×10^3 s implied by aircraft measurements of HCHO and isoprene columns over North America [*Millet et al.*, 2006]. The intercept B (0.5×10^{16} molecules cm^{-2}) is consistent with the lowest columns measured over North America during the INTEX-A aircraft mission [*Millet et al.*, 2006].

[35] Figure 11 shows the relationship between E_{isop} predicted by MEGAN (using both the MDVD2 and CLM land cover databases) and the corresponding HCHO column simulated by GEOS-Chem, computed separately for each model grid square at the satellite overpass time (12:00–15:00 LT). We can only derive a meaningful local slope at locations where the isoprene emissions exceed 2×10^{12} atomsC cm^{-2} s^{-1} (see below), and grid squares not meeting this criterion (according to MEGAN) are grayed out. We also omit grid squares where the $\Omega_{\mathrm{HCHO}} - E_{isop}$ correlation is low ($R < 0.4$); this occurs along the Gulf Coast, where frequent inflow of marine air disrupts the local relationship. The uniform and spatially resolved approaches give consistent slopes where the correlation is high (this includes the dominant isoprene source regions of

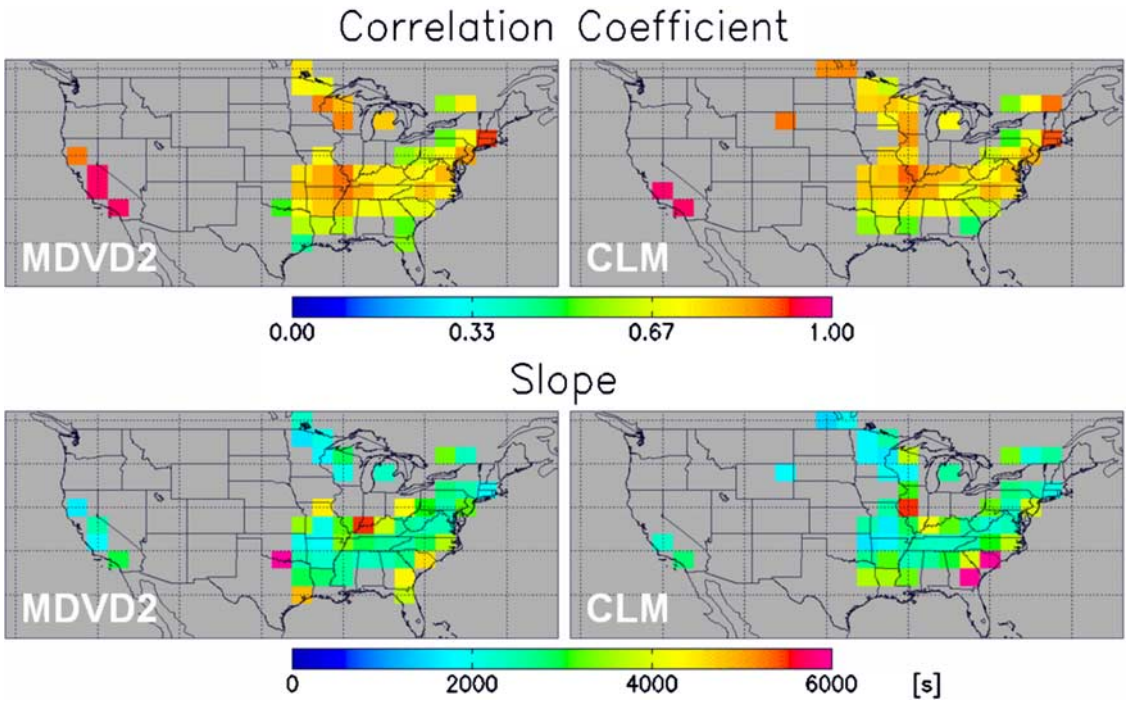

Figure 11. Relationship between HCHO column and isoprene emission at 12:00–15:00 local time computed locally for each 2° × 2.5° GEOS-Chem grid square for June-August 2006. Top panel shows the correlation coefficient (R) and bottom panel shows the slope (*S*) of the reduced major axis regression. We can only derive a meaningful local slope where isoprene emissions exceed 2×10^{12} atomsC cm^{-2} s^{-1}; grid squares not meeting this criterion (according to MEGAN) are grayed out.

the southern and eastern United States): for R > 0.7, the median slopes are 2.5×10^3 s (MDVD2) and 2.4×10^3 s (CLM), with an interquartile (25th–75th percentile) range of $2.0–3.0 \times 10^3$ s. Thus the error associated with assuming a uniform slope is approximately 20%. We see that the local regression method gives anomalously high slopes in a few low-emission locations (e.g., on the Texas-Oklahoma border and in southern Indiana), due to the influence of neighboring high-emission grid cells. The local intercepts (not shown) are consistent between MDVD2 and CLM, and similar to that derived using the uniform approach: for R > 0.7, the median value is 0.4×10^{16} molecules cm^{-2} (both MDVD2 and CLM), with interquartile ranges of $0.2–0.5 \times 10^{16}$ molecules cm^{-2} (MDVD2) and $0.3–0.5 \times 10^{16}$ molecules cm^{-2} (CLM).

[36] *Millet et al.* [2006] previously estimated a 40% error in the inference of local isoprene emissions from HCHO column measurements, taking into account errors in both the retrieval and the $\Omega_{HCHO} - E_{isop}$ relationship. The lower limit of detection for isoprene emission is defined by retrieval noise and by HCHO column variability from factors other than isoprene. The standard deviation in the HCHO column integrated production rate due to non-isoprene precursors, as determined from aircraft measurements, was found by *Millet et al.* [2006] to be 7×10^{11} molecules cm^{-2} s^{-1} over North America in summer. This value divided by the time-integrated HCHO molar yield from isoprene oxidation (1.6; *Millet et al.* [2006]) implies a lower detection limit of 2×10^{12} atomsC cm^{-2} s^{-1} for the isoprene source. The detection limit due to retrieval noise can be estimated from the detection limit of the satellite instrument ($\sim 4 \times 10^{15}$ molecules cm^{-2}) divided by a typical HCHO column lifetime (~2 h; *Palmer et al.* [2003]): 5.6×10^{11} molecules cm^{-2} s^{-1}. Accounting for the HCHO yield from isoprene oxidation, this again is equivalent to an isoprene source of 2×10^{12} atomsC cm^{-2} s^{-1}. Adding these terms in quadrature we estimate our overall detection limit at 3×10^{12} atomsC cm^{-2} s^{-1}.

5. Isoprene Emissions From OMI: Comparison to MEGAN

[37] Figures 12 and 13 show the isoprene emissions (12:00–15:00 local time) derived from OMI (June–August 2006) on a 1° × 1° grid using both the uniform and variable regression methods. Numbers inset show the 24-h average OMI isoprene emissions for the same time period; these are calculated from the 12:00–15:00 values using local diurnal factors from the GEOS-Chem simulation. The slight change in OMI isoprene emissions between the two figures results from using different vegetation databases to derive the $\Omega_{HCHO} - E_{isop}$ conversion factors. With the variable regression method we can only derive isoprene emissions where the $\Omega_{HCHO}-E_{isop}$ slope is well defined; other grid cells are grayed out. The spatial distribution of emissions is generally consistent between the uniform and variable slope approaches, with the highest isoprene emissions in the Deep South and along the southern Atlantic coast of the United States. Isoprene emissions in the western United States are generally at or below the detection limit of 3×10^{12} atomsC cm^{-2} s^{-1}.

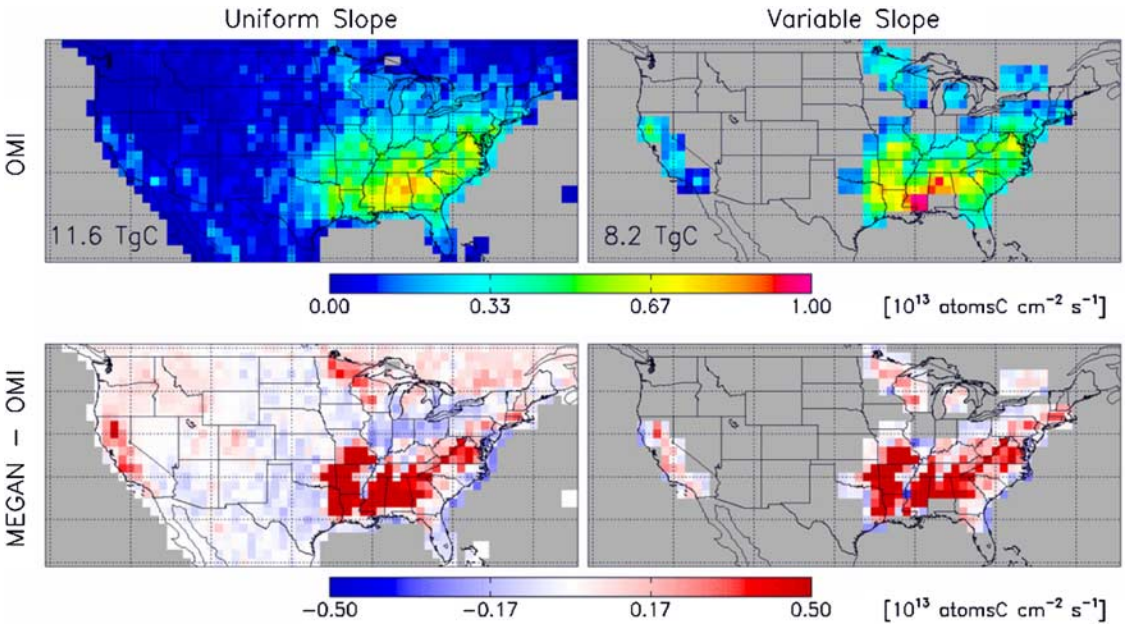

Figure 12. OMI isoprene emissions (June–August 2006) at 12:00–15:00 local time, and difference with MEGAN bottom-up emissions computed using the MDVD2 vegetation database. Numbers inset give total (24-h) OMI isoprene emissions for the same time period. The MEGAN emissions are shown in Figure 6. Conversion of OMI HCHO columns to isoprene emissions was done using the uniform slope approach (left) or the variable slope approach (right). See text for details.

[38] The uniform slope method results in total North American isoprene emissions of 11.6 TgC for June–August 2006. This is 23% lower than the MDVD2-driven MEGAN emissions and 4% lower than the CLM-driven MEGAN emissions. The domain used with the variable slope method is smaller than with the uniform method, and varies depending on whether MDVD2 or CLM is used to define the $\Omega_{HCHO} - E_{isop}$ relationship. In the first case we obtain 8.2 TgC (versus 10.6 TgC predicted by MEGAN over the corresponding domain), and in the second 7.2 TgC (versus 8.6 TgC predicted by MEGAN). Subsampling the uniform slope OMI-derived emissions to the variable slope domain yields similar results: 7.4 TgC (MDVD2) and 7.1 TgC (CLM).

[39] While OMI isoprene emissions, aggregated over the entire domain, are within ~25% of the MEGAN estimates, OMI reveals significant errors in the spatial distribution used in MEGAN. The top two panels of Figure 14 show

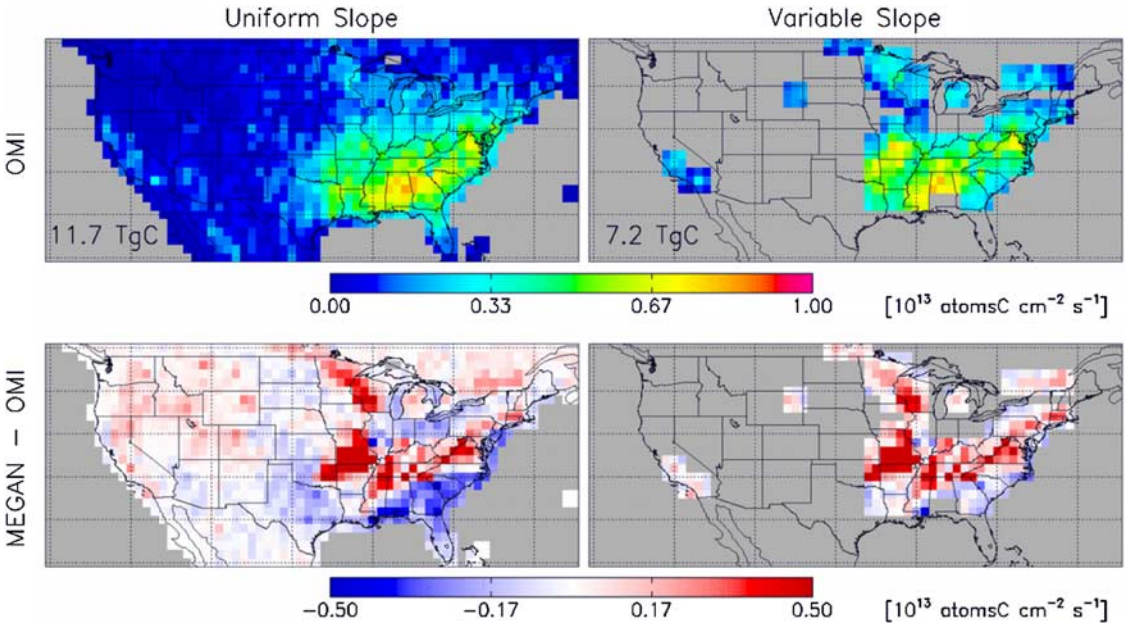

Figure 13. Same as Figure 12 except that MEGAN bottom-up emissions and OMI conversion factors are computed using the CLM vegetation database.

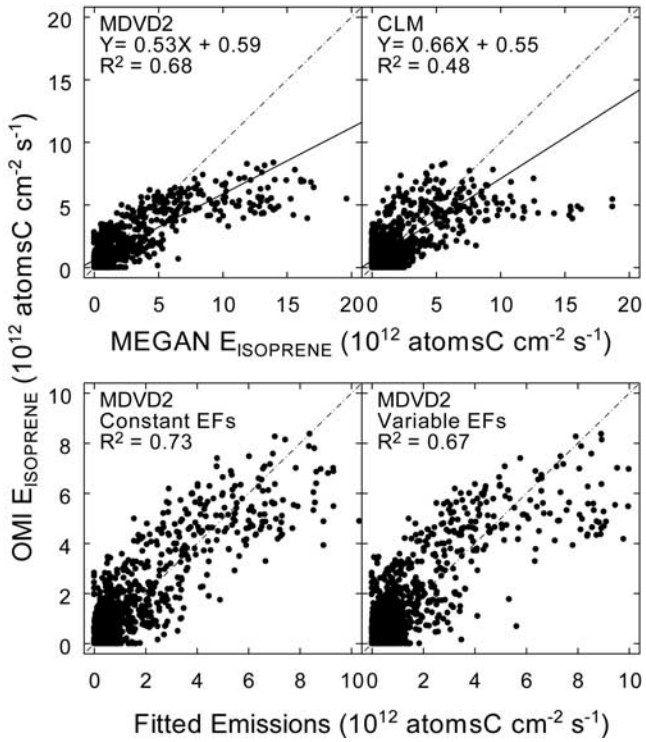

Figure 14. Top panels: OMI versus MEGAN isoprene emissions using either the MDVD2 (left) or CLM (right) vegetation database. The OMI emissions are derived using the uniform slope approach. Bottom panels: results of regressing the OMI isoprene emissions against the broadleaf tree PFT, using uniform emission factors (left) or including MEGAN spatial variability in emission factors (right).

scatterplots of 1° × 1° OMI isoprene emissions (uniform slope method) versus those predicted by MEGAN for both MDVD2 and CLM. The correlation between the OMI and MEGAN emissions (R^2 = 0.48 for CLM and 0.68 for MDVD2) is significantly lower than between the 2° × 2.5° GEOS-Chem and OMI HCHO columns (R^2 = 0.85 and 0.92, shown in Figure 9). Fine-scale variability in emissions, difficult to capture in bottom-up models, gets smoothed out at coarser spatial resolution. We see from the bottom panels of Figures 12 and 13 that these spatial discrepancies are robust across our two methods for calculating isoprene emissions from the OMI HCHO columns.

[40] The vegetation cover used as input to MEGAN covaries to some extent with the surface UV albedos used in the OMI HCHO retrieval, and we carried out a test to determine the impact of this correlation on our results. Using a constant UV albedo (0.03, the domain mean over land) in the OMI HCHO retrieval does not noticeably change the results of Figures 12 and 13, or the regression results shown in the top panels of Figure 14 (slopes change <1%, correlations decrease slightly).

[41] With both the MDVD2 and CLM vegetation, MEGAN overestimates the isoprene flux from three of its most important emission regions: the Ozark Plateau in northern Arkansas and southern Missouri; the Upper South extending from northern Mississippi through Tennessee, Kentucky and the Virginias; and northern Minnesota and western Wisconsin. The high MEGAN emissions in these regions are driven by extensive broadleaf tree cover (Figure 5), and the isoprene emission bias could arise from an overestimate of emissions from this PFT.

[42] When driven by CLM vegetation, MEGAN underestimates isoprene emissions in the Deep South and along the Gulf and southern Atlantic coasts. Conversely, with MDVD2 vegetation, the overestimate in the Upper South extends throughout the Deep South. This disparity is driven by different estimates of broadleaf tree and shrub cover in this region (Figure 5). The MDVD2 database adjusts the AVHRR-derived broadleaf and needleleaf PFT fractions using forest inventory data from the U.S. Forest Service [*Kinnee et al.*, 1997; *Guenther et al.*, 2006]. This adjustment has the greatest impact in the pine plantations of the U.S. Southeast coastal region. While the AVHRR data characterizes these forests as almost entirely needleleaf trees, the ground survey data reveal a significant contribution from broadleaf trees. This is likely due to the dominance of needleleaf trees in the overstory and broadleaf trees in the understory. Thus it appears that the CLM underestimate in the coastal U.S. Southeast is due to insufficient broadleaf tree coverage in that region. On the other hand, fineleaf evergreen trees and crops are also prevalent in the Deep South, and it is possible that isoprene emissions from one or both of these PFTs are underestimated.

6. Implications for Isoprene Emission From Broadleaf Tree Canopies

[43] We now explore the constraints from the OMI observations on the vegetation-specific emission factors used in MEGAN. For this purpose we use MEGAN with MDVD2 land cover, which gives a better correlation with OMI than the CLM land cover (Figure 14). We focus our attention on the broadleaf tree PFT as the dominant isoprene source; emissions from the other PFTs are too low relative to the OMI detection limit to derive robust constraints.

[44] Since the MEGAN EF for a given PFT varies with location, we take two approaches to regressing the OMI isoprene emissions against the broadleaf tree PFT. In the first, we retain the MEGAN EF variability shown in Figure 5, and solve for the factor by which broadleaf tree isoprene emissions should be scaled to best match the OMI observations. EFs for the other PFTs are assumed equal to their original (spatially variable) MEGAN values. In the second approach, we ignore geographic variability in the EFs and solve for the optimum single emission factor for the broadleaf tree PFT. Here the EFs for the other PFTs are set equal to their mean values from MEGAN.

[45] Figure 14 shows the regression results. Given the good agreement between the OMI isoprene emissions derived using the uniform and variable slope methods (Figure 12), we use here the uniform-slope emissions due to greater coverage. Maintaining the spatial distribution of the MEGAN EFs, we obtain the best agreement with OMI (R^2 = 0.67) by scaling the broadleaf tree emissions by 0.56 ± 0.02. The stated uncertainty reflects the standard error of regression computed using jackknife resampling (i.e., subsampling without replacement; [*Manly*, 1997]). This implies 1° × 1° average EFs ranging from 0 to 22 × 10^{12} atomsC cm^{-2} s^{-1} for broadleaf trees over the United

States. We obtain a better fit using uniform emission factors for each PFT ($R^2 = 0.73$; Figure 14). The optimum average EF for the broadleaf tree PFT is then $13.1 \pm 0.4 \times 10^{12}$ atomsC cm^{-2} s^{-1}, similar to the average MEGAN value for the United States (11.8×10^{12} atomsC cm^{-2} s^{-1}), but effectively rejecting the MEGAN use of much higher (3–4×) EFs in certain locations (Figure 5). The fact that the constant-EF approach captures more of the variance in the OMI-derived emissions implies that the extent of EF variability within a given PFT is still poorly constrained by bottom-up estimates, and suggests that isoprene emissions can be more reliably modeled using the simpler uniform-EF approach.

[46] MEGAN EFs largely originate from leaf, branch, and plant enclosure measurements, and one possible explanation for the observed EF discrepancy between OMI and MEGAN is that isoprene or its immediate oxidation products are lost within the forest canopy more rapidly than reflected in current models. Recent measurements over a pine forest [*Farmer and Cohen*, 2008] and the Amazon rain forest [*Kuhn et al.*, 2007] imply high OH levels within the canopy (up to 3×10^7 molecules cm^{-3}). Under such conditions, isoprene oxidation (timescale ~6 min) competes with canopy ventilation (typical timescale ~2–10 min; [*Holzinger et al.*, 2005; *Simon et al.*, 2005; *Farmer and Cohen*, 2008; *Fuentes et al.*, 2007]), so that much of the isoprene emitted below the crown would not escape from the canopy. The HCHO produced within the canopy would then be subject to within-canopy loss from oxidation and deposition. Thus the effective isoprene emission to the atmosphere (as detected by OMI) could be significantly lower than the actual isoprene emission by the vegetation (as described by MEGAN). If true, the curvature seen in Figures 9 and 14 suggests the effect is more pronounced for heavily forested/high emitting canopies.

[47] A second possible explanation for the OMI-MEGAN discrepancy lies with the land cover database. MDVD2 adjusts MODIS vegetation coverage using ground truth data from the United States Forest Service [*Kinnee et al.*, 1997; *Guenther et al.*, 2006], and so should be reliable. However, our work here comparing MDVD2 and CLM highlights the uncertainty in current land cover databases, and it is possible that the EF optimization above partly accounts for errors in the MDVD2 PFT distributions or in the AVHRR LAI database.

7. Conclusions

[48] We presented HCHO column measurements for June–August 2006 over North America from the OMI sensor aboard the Aura satellite launched in 2004, and compared them to previous 1996–2001 measurements from the GOME sensor aboard the ERS-2 satellite. We then used the OMI measurements together with a chemical transport model (GEOS-Chem) to evaluate a state-of-science emission inventory for biogenic isoprene (MEGAN), and to derive new constraints on the isoprene emission capacity of broadleaf trees.

[49] The high spatial resolution of OMI (13×24 km^2 at nadir) relative to GOME (40×320 km^2) and its daily global coverage (vs. three days for GOME) affords improved counting statistics and cloud screening. OMI and GOME are in sun-synchronous orbits with different local overpass times (13:30 for OMI, 10:30 for GOME), but we expect the HCHO column to vary by less than 2% between these two times of day. The OMI spatial distribution over North America in summer is similar to that observed by GOME in previous years ($R^2 = 0.29–0.60$, slope = 0.70–0.92). Both show maxima in the U.S. Southeast but OMI exhibits less retrieval noise. Using temperature to correct for interannual variability we determined that OMI is 2–14% lower than GOME, which is within the estimated systematic retrieval error.

[50] The spatial distribution of HCHO columns observed by OMI is consistent with the emission pattern of isoprene, which represents the main HCHO precursor in North America in summer. Anthropogenic VOC emissions in urban areas are undetectable even with the high resolution of OMI. An exception is Houston where high olefin emissions from the petrochemical industry provide a detectable signal consistent with previous in situ measurements.

[51] Isoprene emissions (E_{isop}) were estimated at $1° \times 1°$ spatial resolution from the OMI measurements of HCHO columns (Ω_{HCHO}) by using $\Omega_{HCHO} - E_{isop}$ relationships from linear regression in the GEOS-Chem model. We used two approaches. The first is based on a single uniform $\Omega_{HCHO} - E_{isop}$ relationship, derived from linear regression over the entire North American domain (65–130°W, 25–50°N); in this case spatial variability in retrieved isoprene emissions is solely determined by the OMI data. The second employs a local $\Omega_{HCHO} - E_{isop}$ relationship specific to each model grid square; in this case the retrieved isoprene emissions contain model information related to local photochemistry and isoprene emission gradients. The two approaches yield consistent $\Omega_{HCHO} - E_{isop}$ slopes ($2.0–3.0 \times 10^3$ s), except in a few locations with strong local emission gradients. Similar slopes were previously derived from in situ observations, lending confidence to the overall approach.

[52] We used the isoprene emissions derived from OMI to evaluate the MEGAN emission inventory driven by two land cover databases (MDVD2 and CLM). These two databases have different patterns of broadleaf tree cover, resulting in significant differences in the spatial distribution of computed isoprene emission. The total June–August isoprene emission for North America derived from OMI is 23% lower than MEGAN using MDVD2 and 4% lower than MEGAN using CLM. The spatial distribution of the OMI-derived emissions at $1° \times 1°$ resolution is highly correlated with MEGAN ($R^2 = 0.68$ using MDVD2, $R^2 = 0.48$ using CLM). We find that MEGAN overestimates isoprene emissions from its dominant source regions including the Ozark Plateau, the Upper South, and the Upper Midwest. With MDVD2, the high bias extends from the Upper South to the Gulf and Atlantic coasts, while with CLM emissions are underestimated in the latter region.

[53] We used regression analysis to explore the constraints from the OMI data on isoprene emission factors, focusing on broadleaf trees as the dominant isoprene source. MEGAN uses geographically variable emission factors from broadleaf trees; fitting the OMI constraints while maintaining this variability requires a uniform 44% decrease of the MEGAN emission factors. Using a uniform emission factor from broadleaf trees provides a better fit to OMI

(R^2 = 0.73) and yields an emission factor close to the MEGAN average. This suggests that MEGAN overestimates emissions in areas where it specifies particularly high emission factors. It is also possible that the effective isoprene emission to the atmosphere as observed by OMI may be lower than the actual isoprene emission determined by MEGAN because of fast isoprene oxidation and HCHO removal within the canopy.

[54] **Acknowledgments.** This work was supported by the NASA Atmospheric Composition Modeling and Analysis Program. DBM and CLH thank the NOAA Climate and Global Change program for postdoctoral fellowships.

References

Abbot, D. S., P. I. Palmer, R. V. Martin, K. V. Chance, D. J. Jacob, and A. Guenther (2003), Seasonal and interannual variability of North American isoprene emissions as determined by formaldehyde column measurements from space, *Geophys. Res. Lett.*, *30*(17), 1886, doi:10.1029/2003GL017336.

Acarreta, J. R., J. F. De Haan, and P. Stammes (2004), Cloud pressure retrieval using the O_2-O_2 absorption band at 477 nm, *J. Geophys. Res.*, *109*(D5), D05204, doi:10.1029/2003JD003915.

Bey, I., D. J. Jacob, R. M. Yantosca, J. A. Logan, B. D. Field, A. M. Fiore, Q. B. Li, H. G. Y. Liu, L. J. Mickley, and M. G. Schultz (2001), Global modeling of tropospheric chemistry with assimilated meteorology: Model description and evaluation, *J. Geophys. Res.*, *106*(D19), 23,073–23,095.

Boersma, K. F., H. J. Eskes, and E. J. Brinksma (2004), Error analysis for tropospheric NO_2 retrieval from space, *J. Geophys. Res.*, *109*, D04311, doi:10.1029/2003JD003962.

Boersma, K. F., et al. (2007), Near-real time retrieval of tropospheric NO_2 from OMI, *Atmos. Chem. Phys.*, *7*, 2103–2118.

Cantrell, C. A., J. A. Davidson, A. H. McDaniel, R. E. Shetter, and J. G. Calvert (1990), Temperature-dependent formaldehyde cross-sections in the near-ultraviolet spectral region, *J. Phys. Chem.*, *94*(10), 3902–3908.

Chance, K. (2002), OMI Algorithm Theoretical Basis Document, Volume IV: OMI Trace Gas Algorithms, http://eospso.gsfc.nasa.gov/eos_homepage/for_scientists/atbd/viewInstrument.php?instrument=13.

Chance, K., P. I. Palmer, R. J. D. Spurr, R. V. Martin, T. P. Kurosu, and D. J. Jacob (2000), Satellite observations of formaldehyde over North America from GOME, *Geophys. Res. Lett.*, *27*(21), 3461–3464.

Chance, K., T. P. Kurosu, and C. E. Sioris (2005), Undersampling correction for array detector-based satellite spectrometers, *Appl. Opt.*, *44*(7), 1296–1304.

Chen, Y. H., and R. G. Prinn (2006), Estimation of atmospheric methane emissions between 1996 and 2001 using a three-dimensional global chemical transport model, *J. Geophys. Res.*, *111*(D10), D10307, doi:10.1029/2005JD006058.

DeFries, R. S., M. C. Hansen, J. R. G. Townshend, A. C. Janetos, and T. R. Loveland (2000), A new global 1-km dataset of percentage tree cover derived from remote sensing, *Global Change Biol.*, *6*(2), 247–254.

Ehhalt, D., and M. Prather (2001), Atmospheric Chemistry and Greenhouse Gases, in *Climate Change 2001: The Scientific Basis*, edited by J. T. Houghton, Y. Ding, D. J. Griggs, M. Noguer, P. J. van der Linden, X. Dai, K. Maskell, and C. A. Johnson, Cambridge Univ. Press, New York, NY.

Environmental Protection Agency (EPA) (2003), EPA NEI 1999 v.1 inventory, http://www.epa.gov/ttn/chief/net/1999inventory.html.

Environmental Protection Agency (EPA) (2007), National Emissions Inventory (NEI) Air Pollutant Emissions Trends Data, http://www.epa.gov/ttn/chief/trends/index.html.

Fang, C. W., R. K. Monson, and E. B. Cowling (1996), Isoprene emission, photosynthesis, and growth in sweetgum (Liquidambar styraciflua) seedlings exposed to short- and long-term drying cycles, *Tree Physiol.*, *16*(4), 441–446.

Farmer, D. K., and R. C. Cohen (2008), Observations of HNO_3, ΣAN, ΣPN and NO_2 fluxes: Evidence for rapid HO_x chemistry within a pine forest canopy, *Atmospheric Chemistry and Physics*, submitted.

Frost, G. J., et al. (2006), Effects of changing power plant NO_x emissions on ozone in the eastern United States: Proof of concept, *J. Geophys. Res.*, *111*, D12306, doi:10.1029/2005JD006354.

Fu, T. M., D. J. Jacob, P. I. Palmer, K. Chance, Y. X. Wang, B. Barletta, D. R. Blake, J. C. Stanton, and M. J. Pilling (2007), Space-based formaldehyde measurements as constraints on volatile organic compound measurements in East and South Asia, *J. Geophys. Res.*, *112*, D06312, doi:10.1029/2006JD007853.

Fuentes, J. D., D. Wang, G. Denhartog, H. H. Neumann, T. F. Dann, and K. J. Puckett (1995), Modeled and field measurements of biogenic hydrocarbon emissions from a Canadian deciduous forest, *Atmos. Environ.*, *29*(21), 3003–3017.

Fuentes, J. D., D. Wang, D. R. Bowling, M. Potosnak, R. K. Monson, W. S. Goliff, and W. R. Stockwell (2007), Biogenic hydrocarbon chemistry within and above a mixed deciduous forest, *J. Atmos. Chem.*, *56*(2), 165–185.

Geron, C. D., A. B. Guenther, and T. E. Pierce (1994), An improved model for estimating emissions of volatile organic compounds from forests in the eastern United States, *J. Geophys. Res.*, *99*(D6), 12,773–12,791.

Goldstein, A. H., S. M. Fan, M. L. Goulden, J. W. Munger, and S. C. Wofsy (1996), Emissions of ethene, propene, and 1-butene by a midlatitude forest, *J. Geophys. Res.*, *101*(D4), 9149–9157.

Goldstein, A. H., M. L. Goulden, J. W. Munger, S. C. Wofsy, and C. D. Geron (1998), Seasonal course of isoprene emissions from a midlatitude deciduous forest, *J. Geophys. Res.*, *103*(D23), 31,045–31,056.

Granier, C., G. Pétron, J. F. Müller, and G. Brasseur (2000), The impact of natural and anthropogenic hydrocarbons on the tropospheric budget of carbon monoxide, *Atmos. Environ.*, *34*(29–30), 5255–5270.

Grinspoon, J., W. D. Bowman, and R. Fall (1991), Delayed onset of isoprene emission in developing velvet bean (*Mucuna* sp.) leaves, *Plant Physiol.*, *97*(1), 170–174.

Guenther, A., et al. (1995), A global model of natural volatile organic compound emissions, *J. Geophys. Res.*, *100*(D5), 8873–8892.

Guenther, A., B. Baugh, G. Brasseur, J. Greenberg, P. Harley, L. Klinger, D. Serca, and L. Vierling (1999), Isoprene emission estimates and uncertainties for the Central African EXPRESSO study domain, *J. Geophys. Res.*, *104*(D23), 30,625–30,639.

Guenther, A., T. Karl, P. Harley, C. Wiedinmyer, P. I. Palmer, and C. Geron (2006), Estimates of global terrestrial isoprene emissions using MEGAN (Model of Emissions of Gases and Aerosols from Nature), *Atmos. Chem. Phys.*, *6*, 3181–3210.

Hansen, M. C., R. S. DeFries, J. R. G. Townshend, M. Carroll, C. Dimiceli, and R. A. Sohlberg (2003), Global percent tree cover at a spatial resolution of 500 meters: First results of the MODIS vegetation continuous fields algorithm, *Earth Interactions*, *7*(10), 1–15.

Harley, P. C., M. E. Litvak, T. D. Sharkey, and R. K. Monson (1994), Isoprene emission from velvet bean leaves: Interactions among nitrogen availability, growth photon flux density, and leaf development, *Plant Physiol.*, *105*(1), 279–285.

Hein, R., P. J. Crutzen, and M. Heimann (1997), An inverse modeling approach to investigate the global atmospheric methane cycle, *Global Biogeochem. Cycles*, *11*(1), 43–76.

Henze, D. K., and J. H. Seinfeld (2006), Global secondary organic aerosol from isoprene oxidation, *Geophys. Res. Lett.*, *33*(9), L09812, doi:10.1029/2006GL025976.

Herman, J. R., and E. A. Celarier (1997), Earth surface reflectivity climatology at 340-380 nm from TOMS data, *J. Geophys. Res.*, *102*(D23), 28,003–28,011.

Holzinger, R., A. Lee, K. T. Paw, and A. H. Goldstein (2005), Observations of oxidation products above a forest imply biogenic emissions of very reactive compounds, *Atmos. Chem. Phys.*, *5*, 67–75.

Houweling, S., F. Dentener, and J. Lelieveld (1998), The impact of nonmethane hydrocarbon compounds on tropospheric photochemistry, *J. Geophys. Res.*, *103*(D9), 10,673–10,696.

Hudman, R. C., et al. (2007), Surface and lightning sources of nitrogen oxides over the Unites States: Magnitudes, chemical evolution, and outflow, *J. Geophys. Res.*, *112*, D12S05, doi:10.1029/2006JD007912.

Jacob, D. J., and S. C. Wofsy (1988), Photochemistry of biogenic emissions over the Amazon forest, *J. Geophys. Res.*, *93*(D2), 1477–1486.

Jacob, D. J., B. D. Field, E. M. Jin, I. Bey, Q. B. Li, J. A. Logan, R. M. Yantosca, and H. B. Singh (2002), Atmospheric budget of acetone, *J. Geophys. Res.*, *107*(D10), 4100, doi:10.1029/2001JD000694.

Jacob, D. J., B. D. Field, Q. B. Li, D. R. Blake, J. de Gouw, C. Warneke, A. Hansel, A. Wisthaler, H. B. Singh, and A. Guenther (2005), Global budget of methanol: Constraints from atmospheric observations, *J. Geophys. Res.*, *110*(D8), D08303, doi:10.1029/2004JD005172.

Jobson, B. T., C. M. Berkowitz, W. C. Kuster, P. D. Goldan, E. J. Williams, F. C. Fesenfeld, E. C. Apel, T. Karl, W. A. Lonneman, and D. Riemer (2004), Hydrocarbon source signatures in Houston, Texas: Influence of the petrochemical industry, *J. Geophys. Res.*, *109*(D24), D24305, doi:10.1029/2004JD004887.

Kesselmeier, J., and M. Staudt (1999), Biogenic volatile organic compounds (VOC): An overview on emission, physiology and ecology, *J. Atmos. Chem.*, *33*(1), 23–88.

Kinnee, E., C. Geron, and T. Pierce (1997), United States land use inventory for estimating biogenic ozone precursor emissions, *Ecol. Appl.*, *7*(1), 46–58.

Koelemeijer, R. B. A., and P. Stammes (1999), Effects of clouds on ozone column retrieval from GOME UV measurements, *J. Geophys. Res.*, *104*(D7), 8281–8294.

Krijger, J. M., M. van Weele, I. Aben, and R. Frey (2007), Technical Note: The effect of sensor resolution on the number of cloud-free observations from space, *Atmos. Chem. Phys.*, *7*(11), 2881–2891.

Kroll, J. H., N. L. Ng, S. M. Murphy, R. C. Flagan, and J. H. Seinfeld (2006), Secondary organic aerosol formation from isoprene photooxidation, *Environ. Sci. Technol.*, *40*(6), 1869–1877.

Kuhn, U., et al. (2007), Isoprene and monoterpene fluxes from Central Amazonian rainforest inferred from tower-based and airborne measurements, and implications on the atmospheric chemistry and the local carbon budget, *Atmos. Chem. Phys.*, *7*, 2855–2879.

Kurosu, T. P. (2007), OMHCHO README FILE, http://www.cfa.harvard.edu/~tkurosu/SatelliteInstruments/OMI/PGEReleases/READMEs/OMHCHO_README.pdf.

Kurosu, T. P., K. Chance, and R. J. D. Spurr (1999), CRAG: Cloud Retrieval Algorithm for the European Space Agency's Global Ozone Monitoring Experiment, in *Proceedings of the European Symposium of Atmospheric Measurements From Space*, pp. 513–521, Eur. Space Agency, Paris.

Lamb, B., A. Guenther, D. Gay, and H. Westberg (1987), A national inventory of biogenic hydrocarbon emissions, *Atmos. Environ.*, *21*(8), 1695–1705.

Lamb, B., D. Gay, H. Westberg, and T. Pierce (1993), A biogenic hydrocarbon emission inventory for the U.S.A. using a simple forest canopy model, *Atmos. Environ.*, *27*(11), 1673–1690.

Lerdau, M. T., and H. L. Throop (1999), Isoprene emission and photosynthesis in a tropical forest canopy: Implications for model development, *Ecol. Appl.*, *9*(4), 1109–1117.

Levelt, P. F., G. H. J. Van den Oord, M. R. Dobber, A. Malkki, H. Visser, J. de Vries, P. Stammes, J. O. V. Lundell, and H. Saari (2006), The Ozone Monitoring Instrument, *IEEE Trans. Geosci. Remote Sens.*, *44*(5), 1093–1101.

Levis, S., C. Wiedinmyer, G. B. Bonan, and A. Guenther (2003), Simulating biogenic volatile organic compound emissions in the Community Climate System Model, *J. Geophys. Res.*, *108*(D21), 4659, doi:10.1029/2002JD003203.

Litvak, M. E., F. Loreto, P. C. Harley, T. D. Sharkey, and R. K. Monson (1996), The response of isoprene emission rate and photosynthetic rate to photon flux and nitrogen supply in aspen and white oak trees, *Plant Cell Environ.*, *19*(5), 549–559.

Loveland, T. R., B. C. Reed, J. F. Brown, D. O. Ohlen, Z. Zhu, L. Yang, and J. W. Merchant (2000), Development of a global land cover characteristics database and IGBP DISCover from 1 km AVHRR data, *Int. J. Remote Sens.*, *21*(6–7), 1303–1330.

Manly, B. F. J. (1997), *Randomization, bootstrap and Monte Carlo methods in biology*, Chapman and Hall, New York.

Marquard, L. C., T. Wagner, and U. Platt (2000), Improved air mass factor concepts for scattered radiation differential optical absorption spectroscopy of atmospheric species, *J. Geophys. Res.*, *105*(D1), 1315–1327.

Martin, R. V., D. D. Parrish, T. B. Ryerson, D. K. Nicks, K. Chance, T. P. Kurosu, D. J. Jacob, E. D. Sturges, A. Fried, and B. P. Wert (2004), Evaluation of GOME satellite measurements of tropospheric NO_2 and HCHO using regional data from aircraft campaigns in the southeastern United States, *J. Geophys. Res.*, *109*, D24307, doi:10.1029/2004JD004869.

Meyer-Arnek, J., A. Ladstatter-Weissenmayer, A. Richter, F. Wittrock, and J. P. Burrows (2005), A study of the trace gas columns O_3, NO_2 and HCHO over Africa in September 1997, *Faraday Discussions*, *130*, 387–405.

Mikaloff Fletcher, S. E., P. P. Tans, L. M. Bruhwiler, J. B. Miller, and M. Heimann (2004), CH4 sources estimated from atmospheric observations of CH4 and its C13/C12 isotopic ratios: 1. Inverse modeling of source processes, *Global Biogeochem. Cycles*, *18*(4), GB4004, doi:10.1029/2004GB002223.

Millet, D. B., et al. (2006), Formaldehyde distribution over North America: Implications for satellite retrievals of formaldehyde columns and isoprene emission, *J. Geophys. Res.*, *111*, D24S02, doi:10.1029/2005JD006853.

Monson, R. K., P. C. Harley, M. E. Litvak, M. Wildermuth, A. B. Guenther, P. R. Zimmerman, and R. Fall (1994), Environmental and developmental controls over the seasonal pattern of isoprene emission from aspen leaves, *Oecologia*, *99*(3-4), 260–270.

Müller, J. F. (1992), Geographical distribution and seasonal variation of surface emissions and deposition velocities of atmospheric trace gases, *J. Geophys. Res.*, *97*(D4), 3787–3804.

Myneni, R. B., R. R. Nemani, and S. W. Running (1997), Estimation of global leaf area index and absorbed PAR using radiative transfer models, *IEEE Trans. Geosci. Remote Sens.*, *35*(6), 1380–1393.

Oleson, K. W., et al. (2004), Technical description of the Community Land Model (CLM), National Center for Atmospheric Research, www.cgd.ucar.edu/tss/clm/distribution/clm3.0/TechNote/CLM_Tech_Note.pdf.

Olivier, J. G. J., and J. J. M. Berdowski (2001), Global emissions sources and sinks, in *The Climate System*, edited by J. Berdowski, R. Guicherit, and B. J. Heij, pp. 33–78, A.A. Balkema/Swets and Zeitlinger, Lisse, The Netherlands.

Olson, D. M., et al. (2001), Terrestrial ecoregions of the worlds: A new map of life on Earth, *Bioscience*, *51*(11), 933–938.

Palmer, P. I., D. J. Jacob, K. Chance, R. V. Martin, R. J. D. Spurr, T. P. Kurosu, I. Bey, R. Yantosca, A. Fiore, and Q. B. Li (2001), Air mass factor formulation for spectroscopic measurements from satellites: Application to formaldehyde retrievals from the Global Ozone Monitoring Experiment, *J. Geophys. Res.*, *106*(D13), 14,539–14,550.

Palmer, P. I., D. J. Jacob, A. M. Fiore, R. V. Martin, K. Chance, and T. P. Kurosu (2003), Mapping isoprene emissions over North America using formaldehyde column observations from space, *J. Geophys. Res.*, *108*(D6), 4180, doi:10.1029/2002JD002153.

Palmer, P. I., et al. (2006), Quantifying the seasonal and interannual variability of North American isoprene emissions using satellite observations of the formaldehyde column, *J. Geophys. Res.*, *111*(D12), D12315, doi:10.1029/2005JD006689.

Parrish, D. D. (2006), Critical evaluation of US on-road vehicle emission inventories, *Atmos. Environ.*, *40*(13), 2288–2300.

Perliski, L. M., and S. Solomon (1993), On the evaluation of air mass factors for atmospheric near-ultraviolet and visible absorption spectroscopy, *J. Geophys. Res.*, *98*(D6), 10,363–10,374.

Pétron, G., P. Harley, J. Greenberg, and A. Guenther (2001), Seasonal temperature variations influence isoprene emission, *Geophys. Res. Lett.*, *28*(9), 1707–1710.

Pierce, T., C. Geron, L. Bender, R. Dennis, G. Tonnesen, and A. Guenther (1998), Influence of increased isoprene emissions on regional ozone modeling, *J. Geophys. Res.*, *103*(D19), 25,611–25,629.

Poisson, N., M. Kanakidou, and P. Crutzen (2000), Impact of non-methane hydrocarbons on tropospheric chemistry and the oxidizing power of the global troposphere: 3-Dimensional modelling results, *J. Atmos. Chem.*, *36*(2), 157–230.

Rasmussen, R. A., and M. A. K. Khalil (1988), Isoprene over the Amazon Basin, *J. Geophys. Res.*, *93*(D2), 1417–1421.

Rasmussen, R. A., and F. W. Went (1965), Volatile organic material of plant origin in the atmosphere, *Proc. Natl. Acad. Sci. U. S. A.*, *53*(1), 215–220.

Rosenstiel, T. N., M. J. Potosnak, K. L. Griffin, R. Fall, and R. K. Monson (2003), Increased CO_2 uncouples growth from isoprene emission in an agriforest ecosystem, *Nature*, *421*(6920), 256–259.

Rosenstiel, T. N., A. L. Ebbets, W. C. Khatri, R. Fall, and R. K. Monson (2004), Induction of poplar leaf nitrate reductase: A test of extrachloroplastic control of isoprene emission rate, *Plant Biol.*, *6*(1), 12–21.

Sharkey, T. D., and F. Loreto (1993), Water stress, temperature, and light effects on the capacity for isoprene emission and photosynthesis of kudzu leaves, *Oecologia*, *95*(3), 328–333.

Sharkey, T. D., and E. L. Singsaas (1995), Why plants emit isoprene, *Nature*, *374*(6525), 769.

Sharkey, T. D., and S. S. Yeh (2001), Isoprene emission from plants, *Annu. Rev. Plant Physiol. Plant Mol. Biol.*, *52*, 407–436.

Shim, C., Y. Wang, Y. Choi, P. I. Palmer, D. S. Abbot, and K. Chance (2005), Constraining global isoprene emissions with Global Ozone Monitoring Experiment (GOME) formaldehyde column measurements, *J. Geophys. Res.*, *110*, D24301, doi:10.1029/2004JD005629.

Simon, E., B. E. Lehmann, C. Ammann, L. Ganzeveld, U. Rummel, F. X. Meixner, A. D. Nobre, A. Araujo, and J. Kesselmeier (2005), Lagrangian dispersion of Rn-222, H_2O and CO_2 within Amazonian rain forest, *Agric. Forest Meteorol.*, *132*(3–4), 286–304.

Stammes, P. (2001), Spectral radiance modelling in the UV-Visible range, in *IRS 2000: Current problems in Atmospheric Radiation*, edited by W. L. Smith and Y. M. Timofeyev, A. Deepak, Hampton VA.

Stokes, N. J., G. M. Terry, and C. N. Hewitt (1998), The impact of ozone, isoprene and propene on antioxidant levels in two leaf classes of velvet bean (Mucuna pruriens L.), *J. Exp. Botany*, *49*(318), 115–123.

Sumner, A. L., et al. (2001), A study of formaldehyde chemistry above a forest canopy, *J. Geophys. Res.*, *106*(D20), 24,387–24,405.

Trainer, M., E. J. Williams, D. D. Parrish, M. P. Buhr, E. J. Allwine, H. H. Westberg, F. C. Fehsenfeld, and S. C. Liu (1987), Models and observations of the impact of natural hydrocarbons on rural ozone, *Nature*, *329*(6141), 705–707.

Turner, D. P., J. V. Baglio, A. G. Wones, D. Pross, R. Vong, B. D. McVeety, and D. L. Phillips (1991), Climate change and isoprene emissions from vegetation, *Chemosphere*, *23*(1), 37–56.

Wang, Y. H., D. J. Jacob, and J. A. Logan (1998), Global simulation of tropospheric O_3-NO_x-hydrocarbon chemistry: 1. Model formulation, *J. Geophys. Res.*, *103*(D9), 10,713–10,725.

Wang, J. S., J. A. Logan, M. B. McElroy, B. N. Duncan, I. A. Megretskaia, and R. M. Yantosca (2004), A 3-D model analysis of the slowdown and interannual variability in the methane growth rate from 1988 to 1997, *Global Biogeochem. Cycles*, *18*(3), GB3011, doi:10.1029/2003GB002180.

Went, F. W. (1960), Organic matter in the atmosphere, and its possible relation to petroleum formation, *Proc. Natl. Acad. Sci. U. S. A.*, *46*(2), 212–221.

Wittrock, F., A. Richter, H. Oetjen, J. P. Burrows, M. Kanakidou, S. Myriokefalitakis, R. Volkamer, S. Beirle, U. Platt, and T. Wagner (2006), Simultaneous global observations of glyoxal and formaldehyde from space, *Geophys. Res. Lett.*, *33*(16), L16804, doi:10.1029/2006GL026310.

Wuebbles, D. J., and K. Hayhoe (2002), Atmospheric methane and global change, *Earth Sci. Rev.*, *57*(3–4), 177–210.

Zimmerman, P. (1979), Testing of hydrocarbon emissions from vegetation, leaf litter and aquatic surfaces and development of a method for compiling biogenic emission inventories, EPA-450-4-70-004, U.S. Environmental Protection Agency, Research Triangle Park, NC.

K. F. Boersma, T.-M. Fu, and D. J. Jacob, Department of Earth and Planetary Sciences and School of Engineering and Applied Sciences, Harvard University, Cambridge, MA 02138, USA.

K. Chance and T. P. Kurosu, Harvard-Smithsonian Center for Astrophysics, Cambridge, MA, USA.

A. Guenther, Atmospheric Chemistry Division, National Center for Atmospheric Research, Boulder, CO, USA.

C. L. Heald, Department of Atmospheric Science, Colorado State University, Fort Collins, CO, USA.

D. B. Millet, Department of Soil, Water and Climate, University of Minnesota, St. Paul, MN, USA. (dbm@umn.edu)